Multichromatic travelling waves for lattice Nagumo equations

Hermen Jan Hupkes [*1], Leonardo Morelli [†1], Petr Stehlík[‡2], and Vladimir Švígler [§2]

[1]Mathematisch Instituut, Universiteit Leiden, P.O. Box 9512, 2300 RA Leiden, The Netherlands
[2]Department of Mathematics and NTIS, Faculty of Applied Sciences, University of West Bohemia, Univerzitní 8, 306 14 Plzeň, Czech Republic

January 22, 2019

Abstract

We discuss multichromatic front solutions to the bistable Nagumo lattice differential equation. Such fronts connect the stable spatially homogeneous equilibria with spatially heterogeneous n-periodic equilibria and hence are not monotonic like the standard monochromatic fronts. In contrast to the bichromatic case, our results show that these multichromatic fronts can disappear and reappear as the diffusion coefficient is increased. In addition, these multichromatic waves can travel in parameter regimes where the monochromatic fronts are also free to travel. This leads to intricate collision processes where an incoming multichromatic wave can reverse its direction and turn into a monochromatic wave.

Keywords: reaction-diffusion equations; lattice differential equations; travelling waves; wave collisions.

MSC 2010: 34A33, 37L60, 39A12

1 Introduction

In this paper we are interested in the Nagumo lattice differential equation (LDE)

$$\dot{u}_j(t) = d\big[u_{j-1}(t) - 2u_j(t) + u_{j+1}(t)\big] + u(1-u)(u-a), \tag{1.1}$$

posed on the one-dimensional lattice $j \in \mathbb{Z}$, for small values of the diffusion-coefficient $d > 0$. This so-called anti-continuum regime features spatially periodic equilibria for (1.1) that can serve as buffer zones between regions of space where the homogeneous stable equilibria $u \equiv 0$ and $u \equiv 1$ dominate the dynamics. Our goal here is to continue the program initiated in [24] where two-periodic patterns and their connection to bichromatic waves were rigorously analyzed.

In particular, we build a classification framework that also allows larger periods to be considered. We also construct so-called multichromatic waves, which connect heterogeneous n-periodic rest-states to each other or their homogeneous counterparts $u \equiv 0$ and $u \equiv 1$. We numerically analyze these multichromatic

[*]hhupkes@math.leidenuniv.nl
[†]leonardo.morelli@gmail.com
[‡]corresponding author, pstehlik@kma.zcu.cz
[§]sviglerv@kma.zcu.cz

waves for $n \in \{3, 4\}$ and show that they exhibit richer behaviour than the bichromatic versions. Indeed, these multichromatic waves can disappear and reappear as the diffusion d is increased. In addition, open sets of parameters (a, d) exist where monochromatic and multichromatic waves can travel simultaneously. This allows us to explore various new types of wave collisions.

Reaction-diffusion systems The LDE (1.1) can be seen as the spatial discretization of the Nagumo PDE

$$u_t = u_{xx} + u(1-u)(u-a) \tag{1.2}$$

onto a uniform grid with node-spacing $h = d^{-1/2}$. This scalar reaction-diffusion PDE can serve as a highly simplified model to describe the interaction between two species or states (described by $u = 0$ and $u = 1$) that compete for dominance in a spatial domain [1]. It admits a comparison principle and can be equipped with a variational structure [20], but it also has a rich global attractor. As such, it has served as a prototype system to investigate many of the key concepts in the field of pattern formation, such as spreading speeds for compact disturbances [42], the existence and stability of travelling waves [19, 36] and other non-trivial entire solutions [31, 43].

The semi-discrete version (1.1) has served as a playground to investigate the impact of the transition from a spatially continuous to a spatially discrete domain. From a mathematical point of view, interesting questions and complications arise due to the broken translational invariance [28]. From the practical point of view, it is highly desirable to be able to incorporate the natural spatial discreteness present in many physical systems such as myelinated nerve fibres [35], meta-materials [7, 8, 39] and crystals [9, 12].

Monochromatic waves Substitution of the travelling wave Ansatz $u(x,t) = \Phi(x - ct)$ into the PDE (1.2) yields the travelling wave ODE

$$-c\Phi' = \Phi'' + \Phi(1-\Phi)(\Phi - a). \tag{1.3}$$

On the other hand, substitution of the discrete analog $u_j(t) = \Phi(j - ct)$ into the LDE (1.1) yields the monochromatic wave equation

$$-c\Phi'(\xi) = d\big[\Phi(\xi-1) - 2\Phi(\xi) + \Phi(\xi+1)\big] + \Phi(\xi)\big(1-\Phi(\xi)\big)\big(\Phi(\xi) - a\big), \tag{1.4}$$

which is a functional differential equation of mixed type (MFDE). We use the term monochromatic here to refer to the fact that each spatial index j follows the same waveprofile Φ. We are specially interested in waves that connect the two stable equilibria $u = 0$ and $u = 1$. In particular, we impose the boundary conditions

$$\Phi(-\infty) = 0, \qquad \Phi(+\infty) = 1. \tag{1.5}$$

The ODE (1.3) with (1.5) can be analyzed by phase-plane analysis [19] (and even solved explicitly) to yield the existence of solutions that increase monotonically and have $\operatorname{sign}(c) = \operatorname{sign}(a - \frac{1}{2})$. These waves have a large basin of attraction [19] and can be used as building blocks to construct and analyze more complicated solutions [42].

More advanced techniques are required to analyze (1.4), but again it is possible to show that non-decreasing solutions exist [29]. However, it is now a very delicate question to determine whether the uniquely determined wavespeed $c = c_{\mathrm{mc}}(a, d)$ satisfies $c_{\mathrm{mc}}(a, d) = 0$ or $c_{\mathrm{mc}}(a, d) \neq 0$. Indeed, the broken translational invariance causes an energy-barrier that must be overcome before waves are able to travel. As such, there is an open region in the (a, d)-plane for which $c_{\mathrm{mc}}(a, d) = 0$ holds; see Fig. 10. This pinning phenomenon is generic [2, 6, 15, 16, 21, 26, 27, 30] but not omnipresent [14, 25] in discrete systems and has received considerable attention.

Bichromatic waves The discrete second derivative allows (1.1) to have a much larger class of equilibrium solutions than the PDE (1.2). For example, two-periodic equilibria of the form

$$u_j = \begin{cases} v & j \text{ is even}, \\ w & j \text{ is odd}. \end{cases} \tag{1.6}$$

can be found by solving the two-component system $G(v, w; a, d) = 0$ given by

$$G(v, w; a, d) = \begin{pmatrix} 2d(w - v) + v(1 - v)(v - a) \\ 2d(v - w) + w(1 - w)(w - a) \end{pmatrix}. \tag{1.7}$$

The variable w can be readily eliminated, leading to a ninth-order polynomial equation for the remaining component v. For $0 < d \ll 1$ this polynomial has nine roots, leading to two stable and four unstable two-periodic equilibria for (1.1) besides the three spatially homogeneous equilibria $\{0, a, 1\}$.

In [24] we performed a full rigorous analysis of this system, which shows that the number of these two-periodic equilibria decreases as $d > 0$ is increased. In particular, there exist two functions $0 < d_s(a) < d_u(a)$ defined for $a \in (0, 1)$ so that the two stable patterns $(v_{\rm bc}, w_{\rm bc})$ and $(w_{\rm bc}, v_{\rm bc})$ collide with two unstable patterns and disappear as d crosses $d_s(a)$. The remaining two unstable patterns subsequently collide with (a, a) as d crosses $d_u(a)$, leaving only the three spatially homogeneous equilibria. We emphasize that all these two-periodic equilibria only exist in the region where monochromatic waves are pinned, i.e. $c_{\rm mc}(a, d) = 0$.

Based on general results in [10] we showed that for $0 < d < d_s(a)$ the system (1.1) admits two types of bichromatic waves

$$u_j(t) = \begin{cases} \Phi_e(j - ct) & j \text{ is even}, \\ \Phi_o(j - ct) & j \text{ is odd}. \end{cases} \tag{1.8}$$

The first class satisfies the lower limits

$$\lim_{\xi \to -\infty} \big(\Phi_e(\xi), \Phi_o(\xi)\big) = (0, 0), \qquad \lim_{\xi \to +\infty} \big(\Phi_e(\xi), \Phi_o(\xi)\big) = (v_{\rm bc}, w_{\rm bc}), \tag{1.9}$$

and has wavespeed $c_{0 \to \rm bc} \geq 0$, while the second class satisfies the upper limits

$$\lim_{\xi \to -\infty} \big(\Phi_e(\xi), \Phi_o(\xi)\big) = (v_{\rm bc}, w_{\rm bc}), \qquad \lim_{\xi \to +\infty} \big(\Phi_e(\xi), \Phi_o(\xi)\big) = (1, 1), \tag{1.10}$$

and has $c_{\rm bc \to 1} \leq 0$. In [24] we showed that there exist two thresholds

$$0 < d_{0 \to \rm bc}(a) \leq d_s(a), \qquad 0 < d_{\rm bc \to 1}(a) \leq d_s(a), \tag{1.11}$$

so that in fact $c_{0 \to \rm bc} > 0$ respectively $c_{\rm bc \to 1} < 0$ holds as d is increased above these thresholds. In addition, for all $a \in (0, 1)$ one or both of the inequalities in (1.11) is strict, indicating the presence of one or more *travelling* bichromatic waves for d sufficiently close to $d_s(a)$.

Numerical results indicate that these two types of bichromatic waves can be glued together via an intermediate buffer zone that displays the two-periodic pattern $(v_{\rm bc}, w_{\rm bc})$. This buffer zone is consumed as the waves move towards each other and eventually collide to form a trapped monochromatic wave; see Figure 8 for the trichromatic analogue.

Bichromatic waves have also been found in several other spatially discrete settings. The results in [5, 40] apply to an anti-diffusion version of (1.1) where $d < 0$. This can reformulated as a two-component problem with positive alternating diffusion coefficients, allowing the general results in [10] to be applied. Several versions of the two-periodic FPU problem are considered in [17, 18, 23]. Using a different palette of techniques, the authors obtain so-called nanopteron solutions, which can have small high-frequency oscillations in their tails. Finally, the two-periodic FitzHugh-Nagumo problem was considered in [37] using a modified spectral-convergence argument.

Multichromatic waves The main purpose of the present paper is to illustrate the novel behaviour that arises for (1.1) when considering wave connections to/from stable n-periodic patterns with $n \geq 3$. Our two main conclusions are that the monotonicity properties described above are no longer valid and that travelling multichromatic waves can co-exist with travelling monochromatic waves. In particular, travelling multichromatic waves can appear, disappear and reappear as $d > 0$ is increased and can collide with other multichromatic waves to form travelling monochromatic waves.

Since the degree of the polynomial that governs the n-periodic equilibria is given by 3^n, it is essential to develop an appropriate classification system to keep track of all the roots and their ordering properties. We develop such a system in this paper, using words from the set $\{\mathtt{o}, \mathtt{a}, \mathtt{1}\}^n$ to track roots that bifurcate off the corresponding sequence of zeroes of the cubic at $d = 0$. The lack of monotonicity with respect to d leads to complications and forces us to allow both parameters (a, d) to vary when tracking roots of a related algebraic problem, unlike in [24]. Although the general theory in [10] also applies to our setting, it is still a challenge to check the conditions in a systematic fashion.

Wave collisions Understanding the interaction between waves is an important topic that is attracting considerable attention, primarily in the spatially continuous setting at present. The so-called weak interaction regime where the waves are far apart is relatively well-understood; see e.g. the exit manifold developed by Wright and Hoffman [22] for the discrete setting and the numerous studies on renormalization techniques for the continuous setting [3, 13, 41].

However, at present there is no general theory to understand strong interactions, where the core of the waves approach each other and deform significantly. Early numerical results by Nishiura and coworkers [33] for the Gray-Scott and a three-component FitzHugh-Nagumo system suggest that the fate of colliding waves (annihilation, combination or scattering) is related to the properties of a special class of unstable solutions called separators. Even the internal dynamics of a single pulse under the influence of essential spectrum (a proxy for the advance of a second wave) can be highly complicated, see e.g. [11] for the (partial) unfolding of a butterfly catastrophe.

Naturally, more information can be obtained in the presence of a comparison principle. Indeed, for the PDE (1.2) one can show that monostable waves can merge to form a bistable wave [31] and that counterpropagating waves can annihilate [32, 43]. If one modifies the nonlinearity to allow more zero-crossings, one can stack waves that connect a chain of equilibria to form so-called propagating terraces [34].

We emphasize that the collisions described in this paper are far richer than those described above for (1.2). This is a direct consequence of the delicate structure of the set of equilibria for (1.1). By exploiting the comparison principle, our hope is that this system can serve as a playground for generating and understanding complicated collision processes.

Organization In §2 we discuss the algebraic problem that n-periodic equilibria must satisfy, develop a naming scheme for its roots and formulate a result concerning the existence of travelling waves. In §3 we discuss trichromatic waves and focus on the fact that for certain values of a three-periodic stable equilibria can disappear and reappear as the diffusion parameter d is increased. We move on to quadrichromatic waves in §4, highlighting the fact that quadrichromatic and monochromatic waves can travel simultaneously in certain parameter regions. This allows us to study various types of wave collisions. Finally, in §5 we prove our main result Theorem 2.2, which establishes the existence of multichromatic waves.

Acknowledgments HJH acknowledges support from the Netherlands Organization for Scientific Research (NWO) (grant 639.032.612). LM acknowledges support from the Netherlands Organization for Scientific Research (NWO) (grant 613.001.304). PS acknowledges the support of the project LO1506 of the Czech Ministry of Education, Youth and Sports under the program NPU I. The authors are grateful to Antonín Slavík for his comments.

2 Multichromatic Root Naming and Ordering

The main focus of this paper is the Nagumo lattice differential equation (LDE)

$$\dot{u}_j(t) = d\big[u_{j-1}(t) - 2u_j(t) + u_{j+1}(t)\big] + g\big(u_j(t);a\big), \qquad j \in \mathbb{Z}, \tag{2.1}$$

in which the parameters (a,d) are taken from the half-strip

$$\mathcal{H} = [0,1] \times [0,\infty) \tag{2.2}$$

and the nonlinearity is given by the cubic

$$g\big(u;a\big) = u(1-u)(u-a). \tag{2.3}$$

Our results focus on n-periodic stationary solutions to (2.1) and the waves that connect them.

In §2.1 we develop a naming system that allows us to partially classify these stationary solutions in an intuitive fashion. We proceed in §2.2 by formulating a result for the existence of waves that uses our naming system to decide which equilibria can be connected. Finally, equivalence classes for these waves are introduced in §2.3 by exploiting the symmetries present in (2.1).

2.1 Equilibrium types

We will write n-periodic equilibria for the LDE (2.1) in the form

$$u_i = \mathrm{u}_{\mathrm{mod}(i,n)} \tag{2.4}$$

for some vector $\mathrm{u} \in \mathbb{R}^n$, where we let the modulo operator take values in

$$\mathrm{mod}(i,n) \in \{1,\dots,n\}. \tag{2.5}$$

We remark that u can be interpreted as a solution of the Nagumo equation posed on a cyclic graph of length n; see [38]. Taking $n \geq 3$ and introducing the nonlinear mapping

$$G(\mathrm{u};a,d) := \begin{pmatrix} d(\mathrm{u}_n - 2\mathrm{u}_1 + \mathrm{u}_2) + g\big(\mathrm{u}_1;a\big) \\ d(\mathrm{u}_1 - 2\mathrm{u}_2 + \mathrm{u}_3) + g\big(\mathrm{u}_2;a\big) \\ \vdots \\ d(\mathrm{u}_{n-1} - 2\mathrm{u}_n + \mathrm{u}_1) + g\big(\mathrm{u}_n;a\big) \end{pmatrix} \in \mathbb{R}^n, \tag{2.6}$$

we see that any such equilibrium must satisfy $G(\mathrm{u};a,d) = 0$.

For any $a \in (0,1)$ and $\mathrm{u} \in \{0,a,1\}^n$, it is easy to see that $G(\mathrm{u};a,0) = 0$ and to confirm that the diagonal matrix

$$D_1 G(\mathrm{u};a,0) = \mathrm{diag}\Big(g'(\mathrm{u}_1;a),\dots,g'\big(\mathrm{u}_n;a\big)\Big) \tag{2.7}$$

has non-zero entries. In particular, the implicit function theorem implies that each of these 3^n roots is part of a smooth one-parameter family of roots that exists whenever $|d|$ is small. In fact, one can track the location of each of these roots as d is increased, up until the point where the root in question disappears by colliding with another root. This procedure forms the heart of the naming scheme that we develop here, which will allow us to refer to different types of roots in an efficient manner.

In particular, we set out to label solutions of the equation $G(\cdot\,;a,d) = 0$ with words w taken from the set $\{\mathfrak{o},\mathfrak{a},\mathfrak{1}\}^n$. We emphasize that we are using the fixed symbol $\mathfrak{a}$ as placeholder for the parameter $a \in (0,1)$, which is allowed to vary. Indeed, for any $\mathrm{w} \in \{\mathfrak{o},\mathfrak{a},\mathfrak{1}\}^n$ we introduce the vector $\mathrm{w}_{|a} \in \mathbb{R}^n$ by writing

$$\big(\mathrm{w}_{|a}\big)_i = \begin{cases} 0 & \text{if } \mathrm{w}_i = \mathfrak{o}, \\ a & \text{if } \mathrm{w}_i = \mathfrak{a}, \\ 1 & \text{if } \mathrm{w}_i = \mathfrak{1}. \end{cases} \tag{2.8}$$

Definition 2.1. Consider a word $\mathrm{w} \in \{\mathfrak{o}, \mathfrak{a}, \mathfrak{1}\}^n$ together with a triplet

$$(\mathrm{u}, a, d) \in [0,1]^n \times (0,1) \times [0,\infty). \tag{2.9}$$

Then we say that u is an equilibrium of type w if there exists a C^1-smooth curve

$$[0,1] \ni t \mapsto \big(\mathrm{v}(t), \alpha(t), \delta(t)\big) \in [0,1]^n \times (0,1) \times [0,\infty) \tag{2.10}$$

so that we have

$$\begin{aligned} (\mathrm{v}, \alpha, \delta)(0) &= (\mathrm{w}_{|a}, a, 0), \\ (\mathrm{v}, \alpha, \delta)(1) &= (\mathrm{u}, a, d), \end{aligned} \tag{2.11}$$

together with

$$G\big(\mathrm{v}(t); \alpha(t), \delta(t)\big) = 0, \qquad \det D_1 G\big(\mathrm{v}(t); \alpha(t), \delta(t)\big) \neq 0 \tag{2.12}$$

for all $0 \leq t \leq 1$.

We note that substituting $t = 1$ in (2.12) shows that indeed $G(\mathrm{u}; a, d) = 0$, justifying the terminology of an equilibrium. In addition, the second requirement in (2.12) allows us to apply the implicit function theorem to conclude that $G(\cdot\,; \tilde{a}, \tilde{d}) = 0$ also has equilibria of type w for all pairs $(\tilde{a}, \tilde{d})$ sufficiently close to (a, d). In particular, these observations allow us to introduce the pathwise connected set

$$\Omega_{\mathrm{w}} = \{(a,d) \in \mathcal{H} : \text{the system } G(\cdot\,; a, d) = 0 \text{ admits an equilibrium of type w}\}, \tag{2.13}$$

which is open in the half-strip $\mathcal{H} = [0,1] \times [0,\infty)$.

We now impose the following conditions on the structure of these sets Ω_{w}. The second of these basically states that the interior of the curve (2.10) can be perturbed freely within Ω_{w} without changing the value of the equilibrium u.

(HΩ1) For any two words $\mathrm{w}_A, \mathrm{w}_B \in \{\mathfrak{o}, \mathfrak{a}, \mathfrak{1}\}^n$ the intersection $\Omega_{\mathrm{w}_A} \cap \Omega_{\mathrm{w}_B}$ is connected.

(HΩ2) Consider any word $\mathrm{w} \in \{\mathfrak{o}, \mathfrak{a}, \mathfrak{1}\}^n$ and any $(a,d) \in \Omega_{\mathrm{w}}$, together with a pair of curves

$$[0,1] \ni t \mapsto (\alpha_A, \delta_A)(t) \in \Omega_{\mathrm{w}}, \qquad [0,1] \ni t \mapsto (\alpha_B, \delta_B)(t) \in \Omega_{\mathrm{w}} \tag{2.14}$$

that have

$$(\alpha_A, \delta_A)(0) = (\alpha_B, \delta_B)(0) = (a, 0), \qquad (\alpha_A, \delta_A)(1) = (\alpha_B, \delta_B)(1) = (a, d). \tag{2.15}$$

Then there exist unique functions

$$[0,1] \ni t \mapsto (\mathrm{v}_A, \mathrm{v}_B)(t) \in \mathbb{R}^n \times \mathbb{R}^n \tag{2.16}$$

so that the triplets $(\mathrm{v}_A, \alpha_A, \delta_A)$ and $(\mathrm{v}_B, \alpha_B, \delta_B)$ both satisfy (2.12) for all $0 \leq t \leq 1$, together with the identities

$$\mathrm{v}_A(0) = \mathrm{v}_B(0) = \mathrm{w}_{|a}, \qquad \mathrm{v}_A(1) = \mathrm{v}_B(1). \tag{2.17}$$

At first glance, the condition (HΩ2) appears to be rather cumbersome to verify in practice. To make this more feasible, it is useful to introduce the set

$$\Gamma = \{(a,d) \in \mathcal{H} : \text{ there exists } u \in \mathbb{R}^n \text{ for which } G(u; a, d) = 0 \text{ and } \det D_1 G(u; a, d) = 0\}, \tag{2.18}$$

which by continuity is a closed subset of $\mathcal{H} = [0,1] \times [0,\infty)$. Let us assume that $\mathcal{H} \setminus \Gamma$ consists of a finite number N_Γ of components $\{V_i\}_{i=1}^{N_\Gamma}$ that are open in $\mathcal{H}$ and *simply connected*. On account of a global

implicit function theorem [4, Thm. 3], there exist non-negative integers $\{m_i\}_{i=1}^{N_\Gamma}$ together with smooth functions

$$\mathrm{u}_{i,j} : V_i \to \mathbb{R}^n, \qquad 1 \le i \le N_\Gamma, \qquad 1 \le j \le m_i \tag{2.19}$$

so that $G(\mathrm{u}_{i,j}(a,d); a, d) = 0$ for each $(a,d) \in V_i$. In addition, $\mathrm{u}_{i,j_1}(a,d) \neq \mathrm{u}_{i,j_2}(a,d)$ whenever $j_1 \neq j_2$ and every solution $G(\cdot; a, d) = 0$ with $(a,d) \in V_i$ can be written in this way.

In this setting, (HΩ2) can be verified by checking which of these functions can be connected continuously through the boundaries of adjacent components. Indeed, (HΩ2) is satisfied if there is no sequence of connections that starts in u_{i,j_1} and ends in u_{i,j_2} for some $1 \le i \le N_\Gamma$ and some pair $1 \le j_1 \neq j_2 \le m_i$.

In any case, writing V_* for the component of $\mathcal{H} \setminus \Gamma$ that contains the horizontal segment $(0,1) \times \{0\}$, (HΩ2) can always be achieved if one replaces Ω_w by subsets of the form

$$\Omega_\mathrm{w}^* = \{(a,d) \in V_* : \text{the system } G(\cdot; a, d) = 0 \text{ admits an equilibrium of type w}\}. \tag{2.20}$$

However, we emphasize that (HΩ2) appears to be valid without this artificial restriction for the regions that we have numerically computed in this paper.

Corollary 2.1. Fix an integer $n \ge 2$ and suppose that (HΩ1) and (HΩ2) both hold. Then for any word $\mathrm{w} \in \{\mathfrak{o}, \mathfrak{a}, \mathfrak{1}\}^n$ there is a smooth function $\mathrm{u}_\mathrm{w} : \Omega_\mathrm{w} \to \mathbb{R}^n$ so that $\mathrm{u}_\mathrm{w}(a,d)$ is the unique equilibrium of type w for the system $G(\cdot\,; a, d) = 0$ for all $(a,d) \in \Omega_\mathrm{w}$. In addition, whenever $(a,d) \in \Omega_{\mathrm{w}_A} \cap \Omega_{\mathrm{w}_B}$ for two distinct words $\mathrm{w}_A, \mathrm{w}_B \in \{\mathfrak{o}, \mathfrak{a}, \mathfrak{1}\}^n$ we have

$$\mathrm{u}_{\mathrm{w}_A}(a,d) \neq \mathrm{u}_{\mathrm{w}_B}(a,d). \tag{2.21}$$

Proof. The first statement is a consequence of (HΩ2) and the implicit function theorem. For the second statement, let us argue by contradiction and assume that both vectors in (2.21) are equal to $\mathrm{u} \in \mathbb{R}^n$. Condition (H$\Omega$1) allows us to pick a path from $(a,0)$ to (a,d) that lies entirely within $\Omega_{\mathrm{w}_A} \cap \Omega_{\mathrm{w}_B}$. Applying (H$\Omega$2) shows that u can be continued as an equilibrium along this path back to both $(\mathrm{w}_A)_{|a}$ and $(\mathrm{w}_B)_{|a}$. However, the implicit function theorem implies that this continuation should be unique. □

We emphasize that our classification scheme only track roots until the first time the associated Jacobian becomes singular and the implicit function theorem can no longer be applied. We will encounter several different types of behaviour at such points. It is possible for two roots to collide and become complex and sometimes even recombine at 'later' parameter values. We will also encounter multi-root collisions where one or more roots survive the collision process. In such cases, we often use an ad-hoc naming system, where we label the emerging branch by reusing or combining the types of the original colliding branches.

2.2 Waves

In this section we focus on wave solutions to (2.1) that connect the n-periodic stationary solutions investigated in the previous section. These so-called multichromatic waves can be written as

$$u_j(t) = \Phi_{\mathrm{mod}(j,n)}(j - ct) \tag{2.22}$$

for some wavespeed $c \in \mathbb{R}$ and $\mathbb{R}^n$-valued waveprofile

$$\Phi = (\Phi_1, \Phi_2, \ldots, \Phi_n) : \mathbb{R} \to \mathbb{R}^n \tag{2.23}$$

that satisfies the boundary conditions

$$\lim_{\xi \to -\infty} \Phi(\xi) = \mathrm{u}_{\mathrm{w}_-}, \qquad \lim_{\xi \to +\infty} \Phi(\xi) = \mathrm{u}_{\mathrm{w}_+} \tag{2.24}$$

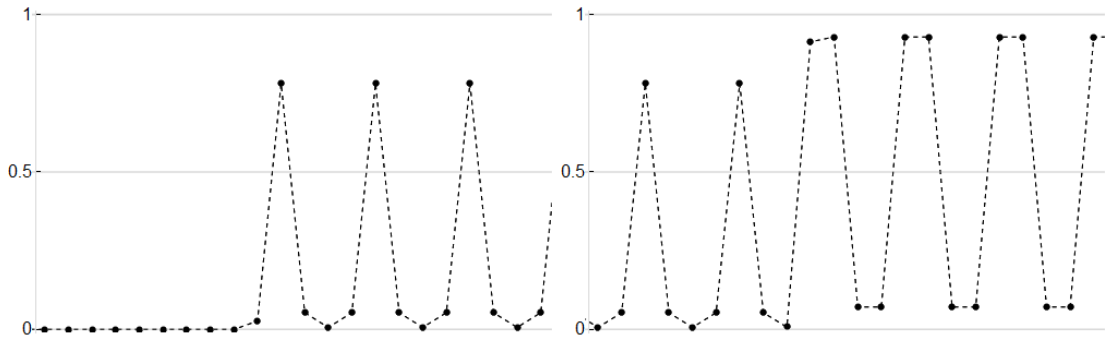

(a) $\mathrm{w}_- = \mathtt{0000}, \mathrm{w}_+ = \mathtt{0001}$. (b) $\mathrm{w}_- = \mathtt{0001}, \mathrm{w}_+ = \mathtt{0011}$.

Figure 1: Two examples of 4-chromatic waves as described in Theorem 2.2.

for some pair of words $\mathrm{w}_\pm \in \{\mathtt{0},\mathtt{1}\}^n$; see Corollary 2.1.

Substituting this Ansatz into (2.1) yields the traveling wave functional differential equation

$$\begin{aligned} -c\Phi_1'(\xi) &= d\big[\Phi_n(\xi-1) - 2\Phi_1(\xi) + \Phi_2(\xi+1)\big] + g\big(\Phi_1(\xi);a\big), \\ -c\Phi_2'(\xi) &= d\big[\Phi_1(\xi-1) - 2\Phi_2(\xi) + \Phi_3(\xi+1)\big] + g\big(\Phi_2(\xi);a\big), \\ &\vdots \\ -c\Phi_n'(\xi) &= d\big[\Phi_{n-1}(\xi-1) - 2\Phi_n(\xi) + \Phi_1(\xi+1)\big] + g\big(\Phi_n(\xi);a\big), \end{aligned} \tag{2.25}$$

which has positive coefficients on all shifted terms and also has diagonal nonlinearities. This system hence fits into the framework developed in [10], provided that the assumptions pertaining to the boundary conditions (2.24) can also be validated.

This is in fact the key question that we address in our main result below. This result requires the following assumption, which states that our root tracking scheme captures all (marginally) stable[1] n-periodic equilibria of the LDE. In particular, the types of these equilibria correspond with words from the *stable* subset $\{\mathtt{0},\mathtt{1}\}^n$.

(HS) Recall the definitions (2.2) and (2.18) and suppose that $G(\mathrm{u};a,d) = 0$ for some $\mathrm{u} \in \mathbb{R}^n$ and $(a,d) \in \mathcal{H}$. Suppose furthermore that all eigenvalues λ of $D_1G(\mathrm{u};a,d)$ satisfy $\lambda \leq 0$. Then we have[2] $\mathrm{u} = \mathrm{u}_\mathrm{w}(a,d)$ for some $\mathrm{w} \in \{\mathtt{0},\mathtt{1}\}^n$ and $(a,d) \in \overline{\Omega}_\mathrm{w}$.

Theorem 2.2 (see §5)**.** *Fix an integer $n \geq 2$ and assume that* (HΩ1)*,* (HΩ2) *and* (HS) *all hold. Consider two distinct words $\mathrm{w}_-, \mathrm{w}_+ \in \{\mathtt{0},\mathtt{1}\}^n$ with $\mathrm{w}_- \leq \mathrm{w}_+$ and pick $(a,d) \in \Omega_{\mathrm{w}_-} \cap \Omega_{\mathrm{w}_+}$ with $d > 0$. Suppose furthermore that one of the following conditions holds.*

(a) The words w_- and w_+ differ at precisely one location.

(b) For each $\mathrm{w} \in \{\mathtt{0},\mathtt{1}\}^n \setminus \{\mathrm{w}_-,\mathrm{w}_+\}$ that satisfies $\mathrm{w}_- \leq \mathrm{w} \leq \mathrm{w}_+$ we have $(a,d) \notin \overline{\Omega}_\mathrm{w}$.

Then there exists a unique $c \in \mathbb{R}$ for which the travelling system (2.25) admits a solution $\Phi : \mathbb{R} \to \mathbb{R}^n$ that satisfies the boundary conditions

$$\lim_{\xi\to-\infty} \Phi(\xi) = \mathrm{u}_{\mathrm{w}_-}(a,d), \qquad \lim_{\xi\to+\infty} \Phi(\xi) = \mathrm{u}_{\mathrm{w}_+}(a,d). \tag{2.26}$$

If $c \neq 0$, then Φ is unique up to translation and each component is strictly increasing.

[1] We use the eigenvalues of the matrix $D_1G(\mathrm{u};a,d)$ to characterize the stability of u. Using the comparison principle this can be easily transferred to the full LDE (1.1).

[2] If $(a,d) \in \partial\Omega_\mathrm{w}$ this identity should be interpreted as a limit.

2.3 Symmetries

There are a number of useful symmetries present in the equilibrium equation $G(\mathrm{u}; a, d) = 0$ and the travelling wave MFDE (2.25). We explore three important transformations here that significantly reduce the number of cases that need to be considered.

We first note that the identity $g(1-u;a) = -g(u;1-a)$ implies that

$$G(\mathbf{1} - \mathrm{u}; a, d) = -G(\mathrm{u}; 1-a, d) \tag{2.27}$$

holds for all $\mathrm{u} \in \mathbb{R}^n$, with $\mathbf{1} = (1, \ldots, 1)^\top \in \mathbb{R}^n$. In order to exploit this, we pick $\mathrm{w} \in \{\mathfrak{0}, \mathfrak{a}, \mathfrak{1}\}^n$ and write $\mathrm{w}_{\mathfrak{0}\leftrightarrow\mathfrak{1}} \in \{\mathfrak{0}, \mathfrak{a}, \mathfrak{1}\}^n$ for the 'inverted' word

$$\big(\mathrm{w}_{\mathfrak{0}\leftrightarrow\mathfrak{1}}\big)_i = \begin{cases} \mathfrak{1} & \text{if } \mathrm{w}_i = \mathfrak{0}, \\ \mathfrak{a} & \text{if } \mathrm{w}_i = \mathfrak{a}, \\ \mathfrak{0} & \text{if } \mathrm{w}_i = \mathfrak{1}. \end{cases} \tag{2.28}$$

The identity (2.27) directly implies the reflection relation

$$\Omega_{\mathrm{w}_{\mathfrak{0}\leftrightarrow\mathfrak{1}}} = \{(a,d) : (1-a, d) \in \Omega_{\mathrm{w}}\}, \tag{2.29}$$

together with

$$\mathrm{u}_{\mathrm{w}_{\mathfrak{0}\leftrightarrow\mathfrak{1}}}(a,d) = \mathbf{1} - \mathrm{u}_{\mathrm{w}}(1-a,d). \tag{2.30}$$

We proceed by introducing the coordinate-shifts $\{T_k\}_{k=1}^n : \mathbb{R}^n \to \mathbb{R}^n$ and reflection $R : \mathbb{R}^n \to \mathbb{R}^n$ that act as

$$\big(T_k \mathrm{u}\big)_i = \mathrm{u}_{\mathrm{mod}(i+k,n)}, \qquad \big(R\mathrm{u}\big)_i = \mathrm{u}_{\mathrm{mod}(1-i,n)}. \tag{2.31}$$

It is easy to verify that the identity $G(\mathrm{u}; a, d) = 0$ implies that also

$$G(T_k\mathrm{u}; a, d) = G(R\mathrm{u}; a, d) = 0. \tag{2.32}$$

In addition, when (c, Φ) is a solution to the travelling wave MFDE (2.25), the same holds for the coordinate-shifted pair $(c, T_k\Phi)$ and the reflected version $(-c, \tilde{\Phi})$ with

$$\tilde{\Phi}(\xi) = R\Phi(-\xi). \tag{2.33}$$

These identities are all consequence of the invariance of the Nagumo LDE (2.1) under the transformations $j \mapsto j + k$ and $j \mapsto -j$.

Our choice to only consider waves where $\Phi(-\infty) \leq \Phi(+\infty)$ breaks the reflection invariance (2.33), which allows us to focus solely on the symmetry caused by the coordinate shifts T_k. In particular, for any word $\mathrm{w} \in \{\mathfrak{0}, \mathfrak{a}, \mathfrak{1}\}^n$, we write

$$\Omega_{[\mathrm{w}]} = \Omega_{\mathrm{w}} = \Omega_{T_1\mathrm{w}} = \ldots = \Omega_{T_{n-1}\mathrm{w}}. \tag{2.34}$$

In addition, we introduce the shorthand notation

$$[\mathrm{w}] = \{\mathrm{u}_{\mathrm{w}}, T_1\mathrm{u}_{\mathrm{w}}, \ldots, T_{n-1}\mathrm{u}_{\mathrm{w}}\} \tag{2.35}$$

to refer to all the roots in the corresponding equivalence class, which are defined for $(a,d) \in \Omega_{[\mathrm{w}]}$.

Note that we are hence treating $[\mathfrak{0a1}]$ and $[\mathfrak{01a}]$ as separate classes, even though they correspond with equivalent equilibria of $G(\cdot; a, d) = 0$. Interestingly enough, when restricting attention to the alphabet $\{\mathfrak{0}, \mathfrak{1}\}^n$, this distinction only plays a role for $n \geq 6$. For example, $\mathfrak{001011}$ is not shift-related to its reflection $\mathfrak{110100}$, but all shorter binary sequences are.

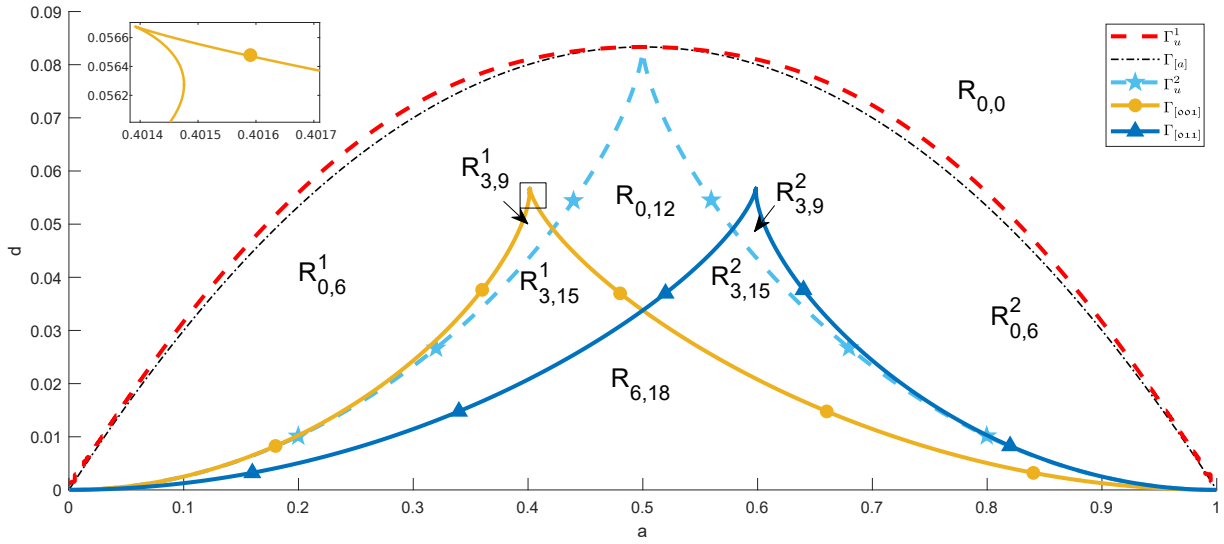

Figure 2: Bifurcation thresholds for the number of roots of (3.1). The subscripts in the regions R indicate the number of stable and unstable roots present in each region, counting their multiplicities but excluding the homogeneous roots $[\mathfrak{o}]$, $[\mathfrak{a}]$ and $[\mathfrak{1}]$.

Whenever we are referring to an equivalence class of roots, we will use the word that is the smallest in the lexicographical[3] sense (the so-called Lyndon word) as a class representative. For example, $\mathfrak{oa11}$ is the Lyndon word for the class

$$[\mathfrak{oa11}] = \{u_{\mathfrak{oa11}}, u_{\mathfrak{1oa1}}, u_{\mathfrak{11oa}}, u_{\mathfrak{a11o}}\}. \tag{2.36}$$

We note that shorter words with a length that divides n can also be interpreted as a word of length n by periodic extension. For example, we write

$$[\mathfrak{o1}] = [\mathfrak{o1o1}] = \{u_{\mathfrak{o1o1}}, u_{\mathfrak{1o1o}}\}. \tag{2.37}$$

For any pair $w_\pm \in \{\mathfrak{o}, \mathfrak{1}\}^n$ with $w_- \leq w_+$, we will use the shorthand notation $u_{w_-} \to u_{w_+}$ to refer to any pair (c, Φ) that satisfies the travelling wave MFDE (2.25) together with the boundary conditions (2.26). The observations above show that $T_k u_{w_-} \to T_k u_{w_+}$ then corresponds with the pair $(c, T_k\Phi)$.

In order to refer to an equivalence class of wave solutions, we pick $w_- \leq w_+$ and introduce the notation

$$[w_- \to w_+] = \{u_{w_-} \to u_{w_+}, T_1 u_{w_-} \to T_1 u_{w_+}, \ldots, T_{n-1} u_{w_-} \to T_{n-1} u_{w_+}\}. \tag{2.38}$$

Here we always take w_- to be the Lyndon representative for its equivalence class, but we emphasize that w_+ *cannot* always be chosen in this way. For example,

$$[\mathfrak{oo1} \to \mathfrak{o11}] = \{u_{\mathfrak{oo1}} \to u_{\mathfrak{o11}}, u_{\mathfrak{1oo}} \to u_{\mathfrak{1o1}}, u_{\mathfrak{o1o}} \to u_{\mathfrak{11o}}\} \tag{2.39}$$

refers to a different set of waves than

$$[\mathfrak{oo1} \to \mathfrak{1o1}] = \{u_{\mathfrak{oo1}} \to u_{\mathfrak{1o1}}, u_{\mathfrak{1oo}} \to u_{\mathfrak{11o}}, u_{\mathfrak{o1o}} \to u_{\mathfrak{o11}}\}. \tag{2.40}$$

Naturally, this distinction disappears when considering waves that connect to or from one of the monochromatic states $[\mathfrak{o}]$ and $[\mathfrak{1}]$.

[3]For ordering purposes we assume that $\mathfrak{o} < \mathfrak{a} < \mathfrak{1}$ holds.

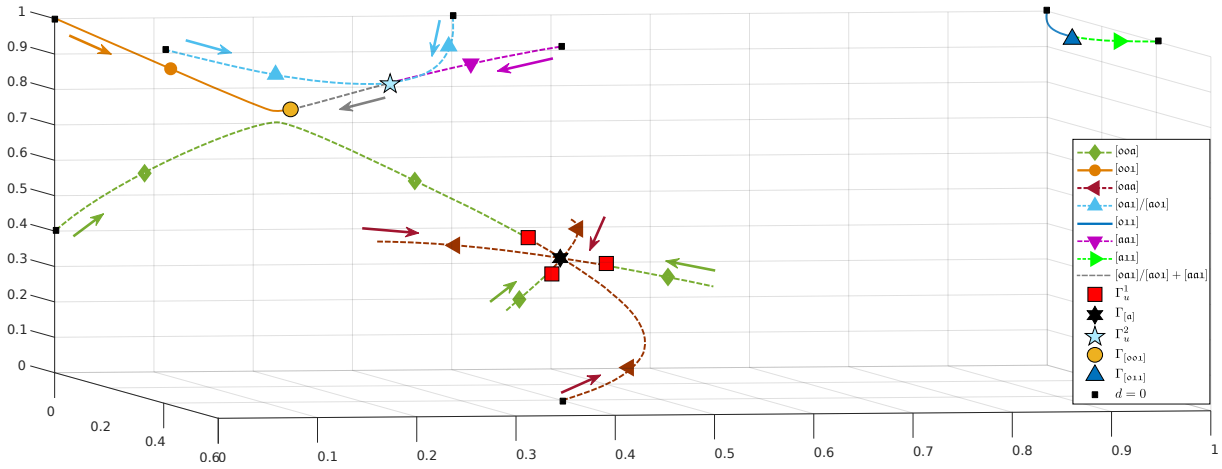

Figure 3: Root trajectories as d is increased for $a = 0.401 < a_c$. The continuous lines represent stable roots branches, while the dashed ones are unstable. In principle only one element of each root class is displayed. However, we (locally) plot all three permutations of $\mathfrak{oaa}$ to show how they all collide with (a, a, a) at $\Gamma_{[\mathfrak{a}]}$ and subsequently pass through each other. Finally, they hit the three permutations of $\mathfrak{oo1}$ at Γ^1_u and disappear. We emphasize that $\mathfrak{ao1}$ is not a Lyndon word, but we need to use it here to describe the Γ^2_u collision.

3 Trichromatic waves

In this section we apply our results to the trichromatic case $n = 3$. As in the bichromatic case considered in [24], we observe that stable 3-periodic equilibria can only exist inside the parameter region where the monochromatic $[\mathfrak{o} \to \mathfrak{1}]$ wave is pinned. The novel behaviour as compared to the bichromatic case is that there exist intervals of the parameter a in which the number of (stable) equilibria can actually increase as d is increased (e.g., for $a = 0.40146$, see Figures 2 and 4). In addition, for values of a in these intervals, there are two disjoint intervals of parameters d for which *travelling* trichromatic waves exist that connect the homogeneous states $[\mathfrak{o}]$ and $[\mathfrak{1}]$ to a stable 3-periodic equilibrium. Similarly, for a fixed d, the number of (stable) equilibria can increase as $\left|a - \frac{1}{2}\right|$ is increased (e.g., for $d = 0.04$, see Figure 2).

3.1 Equilibria

Trichromatic equilibria $\mathrm{u} \in \mathbb{R}^3$ for (2.1) correspond to roots of the nonlinear function

$$G(\mathrm{u}; a, d) = \begin{pmatrix} d(\mathrm{u}_3 - 2\mathrm{u}_1 + \mathrm{u}_2) + g(\mathrm{u}_1; a) \\ d(\mathrm{u}_1 - 2\mathrm{u}_2 + \mathrm{u}_3) + g(\mathrm{u}_2; a) \\ d(\mathrm{u}_2 - 2\mathrm{u}_3 + \mathrm{u}_1) + g(\mathrm{u}_3; a) \end{pmatrix}. \tag{3.1}$$

Inspection of this system shows that one component can be removed if one enforces either $\mathrm{u}_1 = \mathrm{u}_2$, $\mathrm{u}_2 = \mathrm{u}_3$ or $\mathrm{u}_1 = \mathrm{u}_3$.

In Figure 2 we numerically computed the critical set Γ defined in (2.18) by searching for roots of the augmented system

$$G_*(\mathrm{u}; a, d) = \begin{pmatrix} G(\mathrm{u}; a, d) \\ \det D_1 G(\mathrm{u}; a, d) \end{pmatrix}. \tag{3.2}$$

The results show that Γ can be decomposed into 5 piecewise-smooth curves that we label as $\Gamma_{[\mathfrak{a}]}$, $\Gamma_{[\mathfrak{oo1}]}$, $\Gamma_{[\mathfrak{o11}]}$, Γ^1_u and Γ^2_u. The labels of the form $\Gamma_{[\mathrm{w}]}$ imply that $\Gamma_{[\mathrm{w}]} \subset \partial\Omega_{[\mathrm{w}]}$. We emphasize that this naming

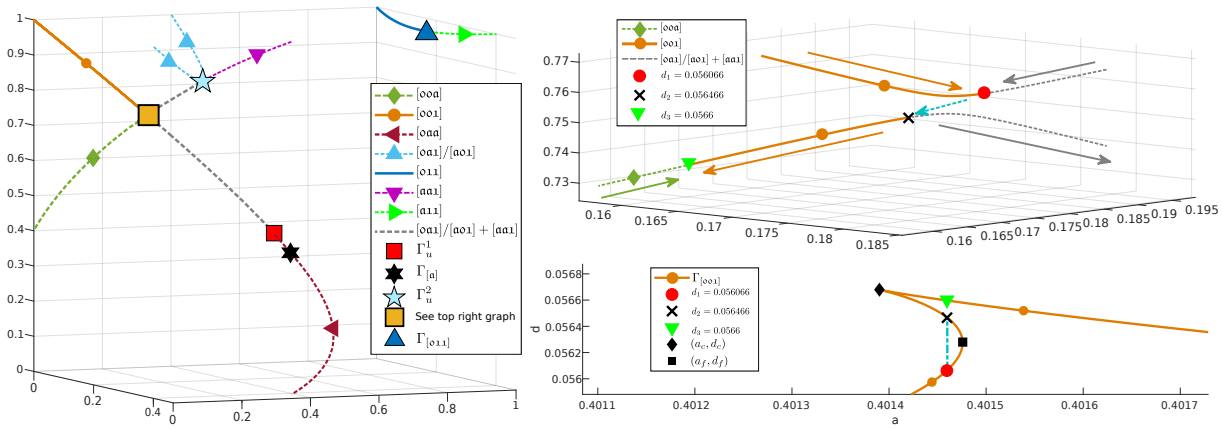

Figure 4: Behaviour of the root branches near the cusp of the yellow $\Gamma_{[\mathfrak{oo1}]}$ curve from Figure 2, which is magnified in the bottom right panel. In particular, we fix $a = 0.40146 \in (a_c, a_f)$ and note that $\Gamma_{[\mathfrak{oo1}]}$ is crossed three times as d is increased. The top right panel contains a zoom of the yellow square from the left panel, which is impacted by these crossings. The blue dashed line between the red circle and black star represents the region where two of the roots are temporarily complex. These plots illustrate the mechanism by which the stable branch $[\mathfrak{oo1}]$ switches its unstable connecting branch as a is increased through the cusp and fold points a_c and a_f.

scheme is ambiguous by its very nature. Indeed, collisions between roots occur precisely on these curves, which also intersect each other.

These 5 curves divide the remaining parameter space $\mathcal{H} \setminus \Gamma$ into 11 open and simply connected components. Ignoring the three homogeneous roots[4] $[\mathfrak{o}]$, $[\mathfrak{a}]$ and $[\mathfrak{1}]$, the bottom region $R_{6,18}$ contains 6 stable roots and 18 unstable roots. The stable roots are represented by the equivalence classes $[\mathfrak{oo1}]$ and $[\mathfrak{o11}]$, while all the remaining equivalence classes generate the unstable roots.

In the discussion below we indicate how this configuration changes as each of the critical curves is crossed. For now, we recall the identity (2.27), which explains the reflection symmetry through the line $a = \frac{1}{2}$ and allows us to focus on the case $a \in (0, \frac{1}{2}]$.

The $\Gamma_{[\mathfrak{o11}]}$ threshold The first threshold that is encountered when increasing d for $a \in (0, \frac{1}{2})$ is the curve $\Gamma_{[\mathfrak{o11}]}$. Here the stable roots $[\mathfrak{o11}]$ collide with the unstable roots $[\mathfrak{a11}]$, after which both branches disappear. This collision is visible in Figures 3, 4 and 5.

In order to find an expansion for this threshold near the corner $(a, d) = (0, 0)$, we exploit the observations above which allow us to consider equilibria close to $(0, 1, 1)$ for which the second and third components are equal. In particular, we construct solutions to the problem

$$G\big((x, 1+y, 1+y); a, d\big) = 0 \tag{3.3}$$

for which $|x| + |y| + |a| + |d|$ is small. The resulting system has a structure that is very similar to that encountered in [24], allowing us to follow the exact same procedure to unfold the saddle node bifurcations. In particular, viewing $\Gamma_{[\mathfrak{o11}]}$ locally as the graph of the function $d_{[\mathfrak{o11}]}$, we obtain the expansion

$$d_{[\mathfrak{o11}]}(a) = \frac{a^2}{8} + \frac{a^4}{64} + O(a^5), \tag{3.4}$$

[4]In the current trichromatic context, these roots are given by $(0, 0, 0)$, (a, a, a) and $(1, 1, 1)$.

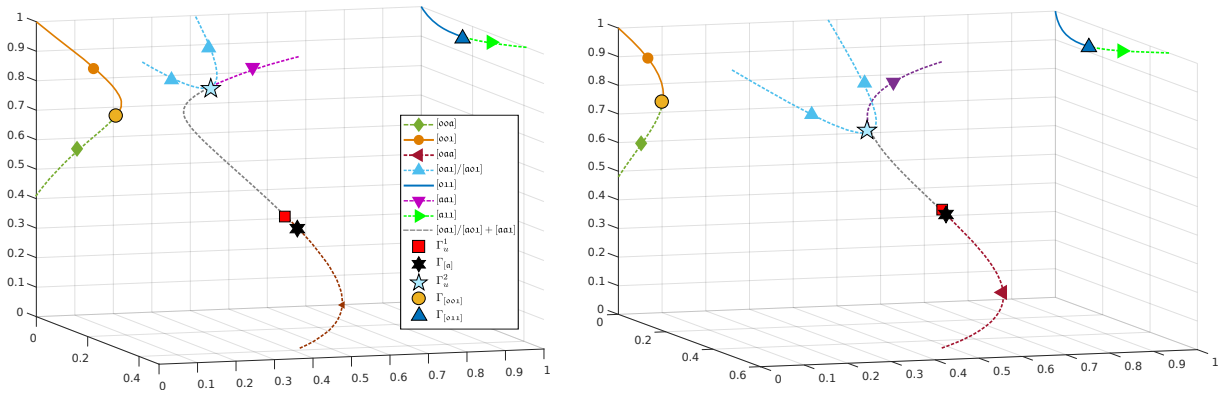

Figure 5: Root branches for $a = 0.41 > a_f$ (left) and $a = 0.48 > a_f$ (right). The branch $[\mathfrak{oo1}]$ now collides with $[\mathfrak{ooa}]$, while the unstable branch spawned by the Γ_u^2 collision collides with $[\mathfrak{oaa}]$ at Γ_u^1. The collision points Γ_u^1 and Γ_u^2 slide through (a, a, a) as a is increased beyond $a = \frac{1}{2}$.

together with

$$\mathrm{u}_{011}\big(a; d_{[\mathfrak{o11}]}(a)\big) = \big(\frac{a}{2}, 1 - \frac{a^2}{8} - \frac{a^3}{16} - \frac{a^4}{64}, 1 - \frac{a^2}{8} - \frac{a^3}{16} - \frac{a^4}{64}\big) + O(a^5). \tag{3.5}$$

The Γ_u^2 threshold This curve features the triple collision of the unstable branches $[\mathfrak{oa1}]$, $[\mathfrak{ao1}]$ and $[\mathfrak{aa1}]$ when $a \in (0, \frac{1}{2})$. One unstable branch of roots emerges from this collision. This collision is visible in Figures 3, 4 and 5.

The $\Gamma_{[\mathfrak{oo1}]}$ threshold The important feature of this curve is that d cannot be expressed as a function of a. Indeed, the function

$$G_{**}(\mathrm{u}; a, d) = \begin{pmatrix} G_*(\mathrm{u}; a, d) \\ \det D_{1,3} G_*(\mathrm{u}; a, d) \end{pmatrix} \tag{3.6}$$

has the (numerically computed) roots

$$(a_c, d_c) \approx (0.4013889, 0.05668), \qquad (a_f, d_f) \approx (0.401476, 0.056275), \tag{3.7}$$

which correspond with a cusp respectively fold point for the curve $\Gamma_{[\mathfrak{oo1}]}$; see Figures 2 and 4.

When $a \in (0, a_c)$, the root $[\mathfrak{oo1}]$ hits the branch spawned by the Γ_u^2 collision and disappears; see Figure 3. On the other hand, for $a \in (a_f, 1)$ the root $[\mathfrak{oo1}]$ hits $[\mathfrak{ooa}]$; see Figure 5. This corresponds with the scenario described above for $\Gamma_{[\mathfrak{o11}]}$ after applying the $\mathfrak{o} \leftrightarrow \mathfrak{1}$ swap.

The intermediate case $a \in (a_c, a_f)$ is illustrated in Figure 4. In this case the root $[\mathfrak{oo1}]$ again hits the branch spawned by the Γ_u^2 collision and disappears, but this pair reappears and splits off from each other after d crosses the $\Gamma_{[\mathfrak{oo1}]}$ threshold a second time. The stable branch of this pair collides with $[\mathfrak{ooa}]$ and disappears when d crosses $\Gamma_{[\mathfrak{oo1}]}$ for the third and final time, while the unstable branch emerges as the survivor of the full triple crossing process.

The black star and green triangle in Figure 4 overlap when $a = a_c$, in which case the $[\mathfrak{ooa}]$ branch has a triple root at the critical value $d = d_c$. On the other hand, the black star and red circle in this figure overlap when $a = a_f$, in which case the branch $[\mathfrak{oo1}]$ and the branch spawned by the Γ_u^2 collision can be said to bounce off each other at $d = d_f$.

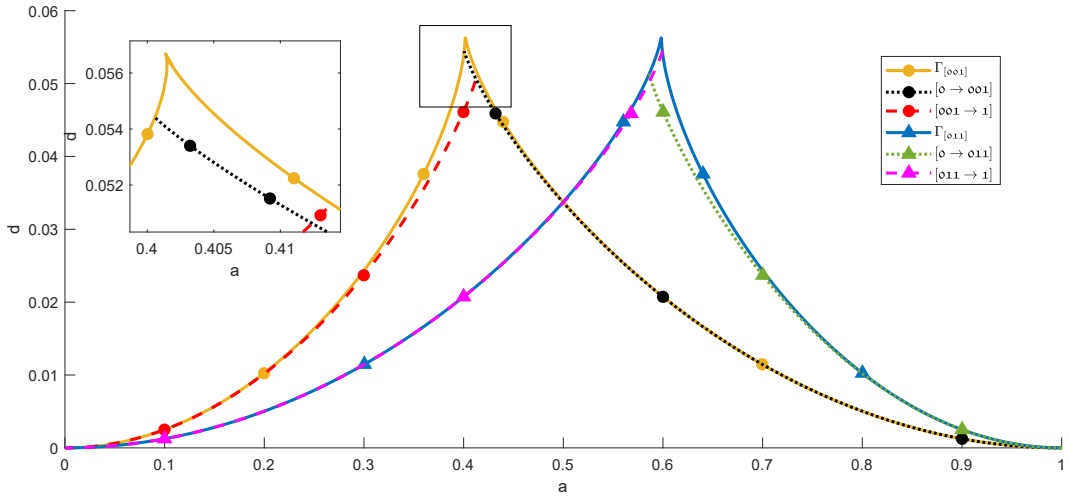

Figure 6: Thresholds where standing waves ($c = 0$) transition to travelling waves ($c \neq 0$) for the connections to and from the homogeneous equilibria $[\mathfrak{o}]$ and $[\mathfrak{1}]$.

In order to find an expansion for this threshold near the corner $(a, d) = (0, 0)$, we now look for solutions to

$$G\big((x, x, 1 + y); a, d\big) = 0 \tag{3.8}$$

for which $|x| + |y| + |a| + |d|$ is small. Viewing $\Gamma_{[\mathfrak{o}\mathfrak{o}\mathfrak{1}]}$ locally as the graph of the function $d_{[\mathfrak{o}\mathfrak{o}\mathfrak{1}]}$, we may again use the same procedure as in [24] to obtain the expansion

$$d_{[\mathfrak{o}\mathfrak{o}\mathfrak{1}]}(a) = \frac{a^2}{4} + \frac{a^4}{8} + O(a^5), \tag{3.9}$$

together with

$$\mathrm{u}_{001}\big(a; d_{[\mathfrak{o}\mathfrak{o}\mathfrak{1}]}(a)\big) = \big(\frac{a}{2}, \frac{a}{2}, 1 - \frac{a^2}{8} - \frac{a^3}{16} - \frac{a^4}{64}\big) + O(a^5). \tag{3.10}$$

The $\Gamma_{[a]}$ threshold This curve is characterized by the relation $\det D_1 G([\mathfrak{a}]; a, d) = 0$, which can be explicitly solved to yield $d_{[\mathfrak{a}]}(a) = a(1-a)/3$. As shown in Figure 3, the three branches of roots contained in the equivalence class $[\mathfrak{o}\mathfrak{a}\mathfrak{a}]$ all pass through (a, a, a) at $d = d_{[\mathfrak{a}]}$ and survive the collision.

The Γ^1_u threshold On this threshold the unstable branch that survived the Γ^2_u and $\Gamma_{[\mathfrak{o}\mathfrak{o}\mathfrak{1}]}$ collisions hits the branch $[\mathfrak{o}\mathfrak{a}\mathfrak{a}]$ that passed through (a, a, a); see Figures 3, 4, 5. Above this threshold the only remaining equilibria are the homogeneous states $[\mathfrak{o}]$ $[\mathfrak{a}]$ and $[\mathfrak{1}]$.

The critical case $a = \frac{1}{2}$ The right panel in Figure 5 describes the situation just before a reaches the critical value $a = \frac{1}{2}$. Upon increasing a through this value, the collisions at Γ^2_u and Γ^1_u both cross through the center $(\frac{1}{2}, \frac{1}{2}, \frac{1}{2})$ at $a = \frac{1}{2}$ and $d = d_{[a]}(\frac{1}{2}) = \frac{1}{12}$, transitioning to occur on the $[\mathfrak{o}\mathfrak{a}\mathfrak{a}]$ branch.

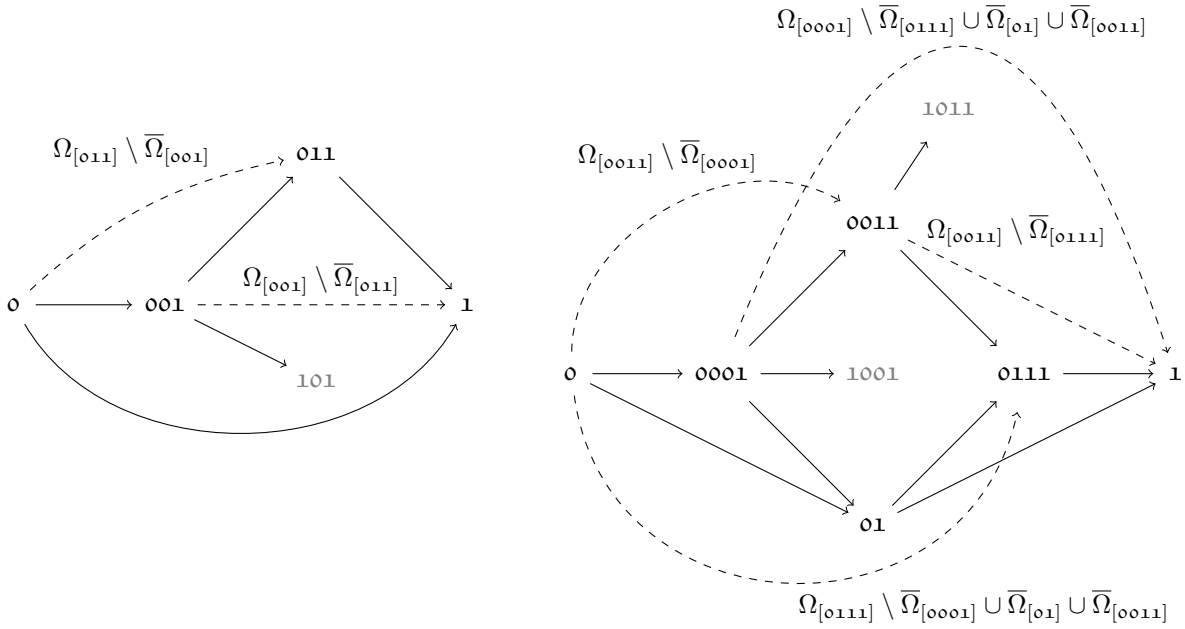

Figure 7: This diagram depicts the trichromatic (left) and quadrichromatic (right) wave connections predicted by the theory in §2. A solid edge from w_- to w_+ indicates that waves of type $[w_- \to w_+]$ exist for $(a, d) \in \Omega_{[w_+]} \cap \Omega_{[w_-]}$ with $d > 0$ by applying Theorem 2.2 with option (a). A dashed edge indicates that this connection is covered by option (b). In this case, the connection is only guaranteed to exist in the parameter region displayed next to the edge, because intermediate stable roots have to be ruled out. The asymptotics in §3.1 and §4.1 guarantee that all the relevant parameter regions are non-empty. In addition, the connections $[0001 \to 1101]$, $[0001 \to 0111]$ and $[0001 \to 1011]$ are not listed because $\Omega_{[0001]} \cap \Omega_{[0111]}$ is contained in $\Omega_{[0011]}$. To prevent clutter, we have also left out the monochromatic $[0 \to 1]$ connection in the diagram on the right. The words that are gray are *not* Lyndon words and as such do not have any outgoing arrows; see the discussion in §2.3.

3.2 Wave Connections

Our numerical results strongly suggest that (HΩ1), (HΩ2) and (HS) are satisfied, allowing us to apply the results in §2. Figure 7 represents the equivalence classes of wave connections between neighbouring words. We note that we are not drawing an edge from 101 because this is not a Lyndon word.

We recall that Theorem 2.2 does not provide any information about the speed c of the travelling wave. We therefore resorted to numerics to find parameter values where $c \neq 0$ for the waves discussed in the diagram above. This was done by connecting the two endstates with a tanh profile and letting this initial profile evolve under the flow of (2.1). Exploiting the stability of the moving waves, one can test whether $c = 0$ by determining whether movement ceases after an initial transient period.

For the $[001 \to 011]$ and $[001 \to 101]$ connections we were not able to find any regions where $c \neq 0$. However, in Figure 6 we can observe the numerically computed minimum threshold for d where we in fact have $c \neq 0$ for the waves that connect to and from the homogeneous states $[0]$ and $[1]$. Notice that both types of waves have non-zero speed in the region around the fold and cusp points of $\Gamma_{[001]}$. This indicates that travelling waves can appear and disappear twice as the diffusion coefficient is increased,

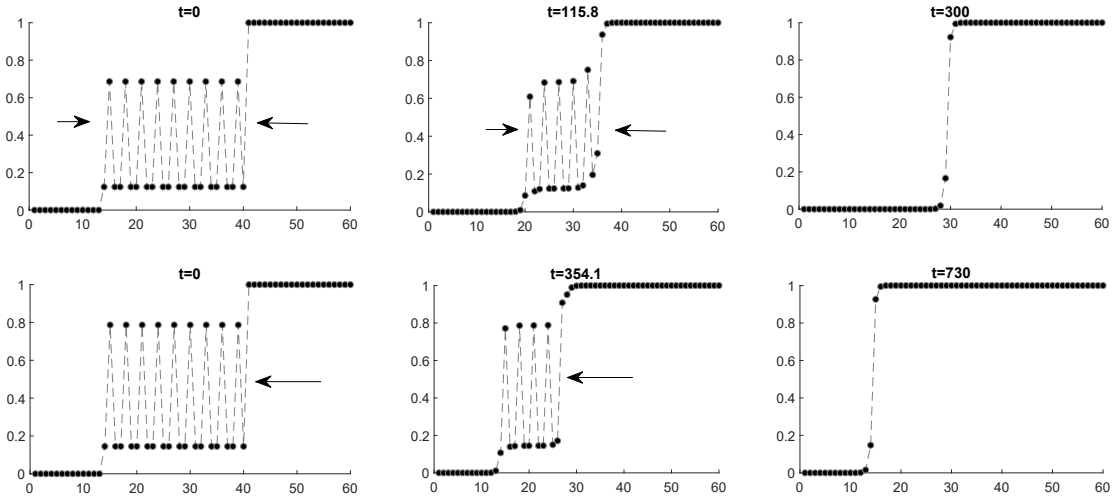

Figure 8: These panels describe two simulations of the LDE (2.1) that feature a collision between a $[\mathtt{0} \to \mathtt{001}]$ wave and a $[\mathtt{001} \to \mathtt{1}]$ wave. For the top three panels we have $a = 0.404$ and $d = 0.054$, which is above both trichromatic speed thresholds. However, it is still below the monochromatic threshold. In particular, the buffer zone is now consumed from both sides, but the end result is again a pinned monochromatic front. For the bottom three panels we have $a = 0.404$ and $d = 0.05$, which is now below the $[\mathtt{0} \to \mathtt{001}]$ but above the $[\mathtt{001} \to \mathtt{1}]$ speed thresholds. Here the $[\mathtt{001}]$ buffer zone is consumed from the right, resulting in a pinned monochromatic front.

which does not happen in the bichromatic case.

In Figure 8 we give snapshots of the collision process that occurs as a $[\mathtt{0} \to \mathtt{001}]$ wave collides with a $[\mathtt{001} \to \mathtt{1}]$ wave. In both cases an intermediate buffer-zone consisting of the trichromatic state $[\mathtt{001}]$ is consumed by one (or both) of the incoming trichromatic waves, leading eventually to a pinned monochromatic wave. This type of collision can also be observed in the bichromatic setting.

4 Quadrichromatic waves

In this section we discuss the quadrichromatic case $n = 4$. As in the trichromatic case, stable 4-periodic equilibria can disappear and reappear as d is increased for a fixed a. The novel behaviour in this setting is that *travelling* quadrichromatic waves can co-exist with *travelling* monochromatic waves for an open set of parameters (a, d). This allows several new types of collisions to occur. For example, two incoming connections with intermediate quadrichromatic states can collide to form a monochromatic travelling wave.

4.1 Equilibria

The relevant nonlinearity that governs quadrichromatic equilibria to (2.1) is now given by

$$G(\mathrm{u}; a, d) := \begin{pmatrix} d(\mathrm{u}_4 - 2\mathrm{u}_1 + \mathrm{u}_2) + g\big(\mathrm{u}_1; a\big) \\ d(\mathrm{u}_1 - 2\mathrm{u}_2 + \mathrm{u}_3) + g\big(\mathrm{u}_2; a\big) \\ d(\mathrm{u}_2 - 2\mathrm{u}_3 + \mathrm{u}_4) + g\big(\mathrm{u}_3; a\big) \\ d(\mathrm{u}_3 - 2\mathrm{u}_4 + \mathrm{u}_1) + g\big(\mathrm{u}_4; a\big) \end{pmatrix}. \tag{4.1}$$

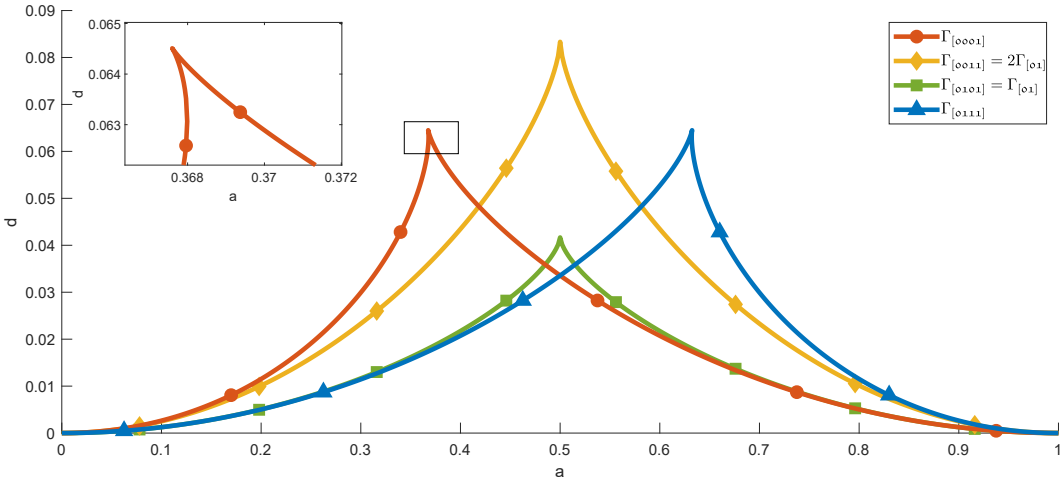

Figure 9: Bifurcation thresholds for the four stable quadrichromatic root classes. The $\Gamma_{[0001]}$ and $\Gamma_{[0111]}$ curves again feature slanted cusps; see the inset.

Inspecting this system shows that one component can be removed by enforcing either $u_1 = u_3$ or $u_2 = u_4$. Of course, this problem reduces to the bichromatic case $n = 2$ if both these identities are enforced. On the other hand, if one takes

$$u_1 = u_2 = u_A, \qquad u_3 = u_4 = u_B, \tag{4.2}$$

the system $G(u; a, d) = 0$ reduces to

$$d(u_B - u_A) + g(u_A; a) = d(u_A - u_B) + g(u_B; a) = 0. \tag{4.3}$$

This again corresponds to the bichromatic case $n = 2$ but now with the halved diffusion coefficient $d_{bc} = \frac{1}{2}d$.

In Figure 9 we display several numerically computed curves $\Gamma_{[w]}$ in the critical set Γ that correspond with the upper boundaries of the sets $\Omega_{[w]}$. For visual clarity, we only consider the words

$$w \in \{0001, 0011, 01, 0111\}, \tag{4.4}$$

which correspond with the stable non-homogeneous equilibria for $G(u; a, d) = 0$.

The curves $\Gamma_{[0001]}$ and $\Gamma_{[0111]}$ again contain cusp and fold points. However, all four curves can *locally* be described as a graph $d = d_{[w]}(a)$ near the corner $(a, d) = (0, 0)$. We now set out to compute the first two terms in the asymptotic expansion of each of these curves.

The $\Gamma_{[0111]}$ threshold In view of the symmetries discussed above we consider solutions where the second and fourth component are equal. In particular, we consider the problem

$$G\big((x, 1 + y, 1 + z, 1 + y); a, d\big) = 0, \tag{4.5}$$

which can be written as

$$(H_1, H_2, H_3)(x, y, z; a, d) = 0 \tag{4.6}$$

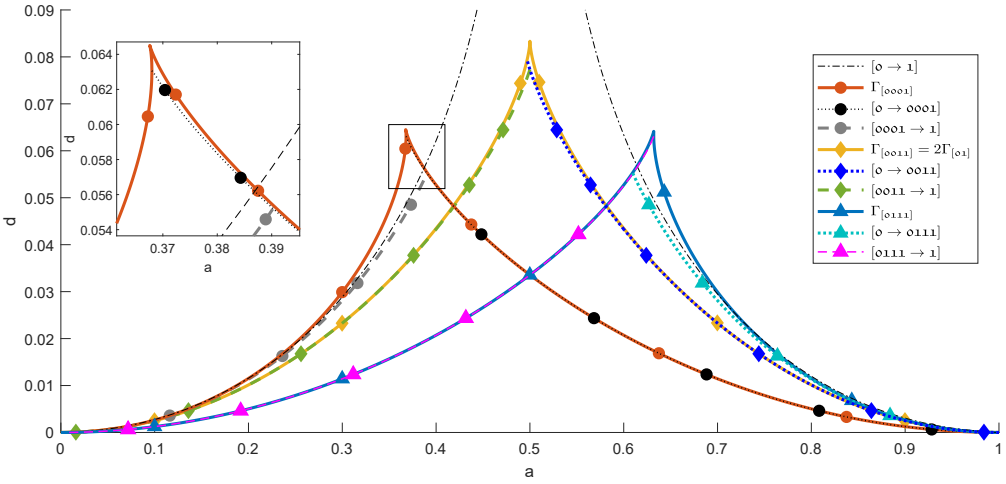

Figure 10: Speed thresholds for the wave connections to and from the stable roots [0001], [0011] and [0111]. The thresholds for [0101] are not shown, as they coincide with the bichromatic results obtained in [24].

with

$$\begin{aligned} H_1(x,y,z;a,d) &= 2d(1+y-x)+x(1-x)(x-a), \\ H_2(x,y,z;a,d) &= d(x+z-2y-1)-y(1+y)(y+1-a), \\ H_3(x,y,z;a,d) &= 2d(y-z)-z(1+z)(z+1-a). \end{aligned} \tag{4.7}$$

Notice that H_2 and H_3 feature terms of order $O(y)$ respectively $O(z)$, which corresponds with the fact that the root $g(1;a) = 0$ is simple when $a = 0$. In addition, H_3 is independent of x. Setting $H_3 = 0$ hence allows us to write $z = z_*(y;a,d)$, which can be substituted into $H_2 = 0$ to yield $y = y_*(x;a,d)$. Plugging these expressions into H_1 by writing

$$\tilde{H}_1(x;a,d) = H_1\big(x, y_*(x;a,d), z_*(y;a,d);a,d\big), \tag{4.8}$$

we find

$$\tilde{H}_1(x;a,d) = x^2 + O\big(x^3 + ax + d\big). \tag{4.9}$$

This allows us to uncover the saddle-node bifurcations in a fashion analogous to [24]. In particular, we obtain the expansion

$$d_{[0111]}(a) = \frac{a^2}{8} + \frac{a^4}{64} + O(a^5), \tag{4.10}$$

together with

$$\mathrm{u}_{0111}\big(a; d_{[0111]}(a)\big) = \big(\frac{a}{2}, 1 - \frac{a^2}{8} - \frac{a^3}{16}, 1, 1 - \frac{a^2}{8} - \frac{a^3}{16}\big) + O(a^4). \tag{4.11}$$

The $\Gamma_{[0101]} = \Gamma_{[01]}$ threshold The discussion above implies that this threshold is identical to the corresponding threshold for the bichromatic case $n = 2$. We can hence copy the results from [24, Prop 3.6] and write

$$d_{[01]}(a) = \frac{a^2}{8} + \frac{a^4}{32} + O(a^5), \tag{4.12}$$

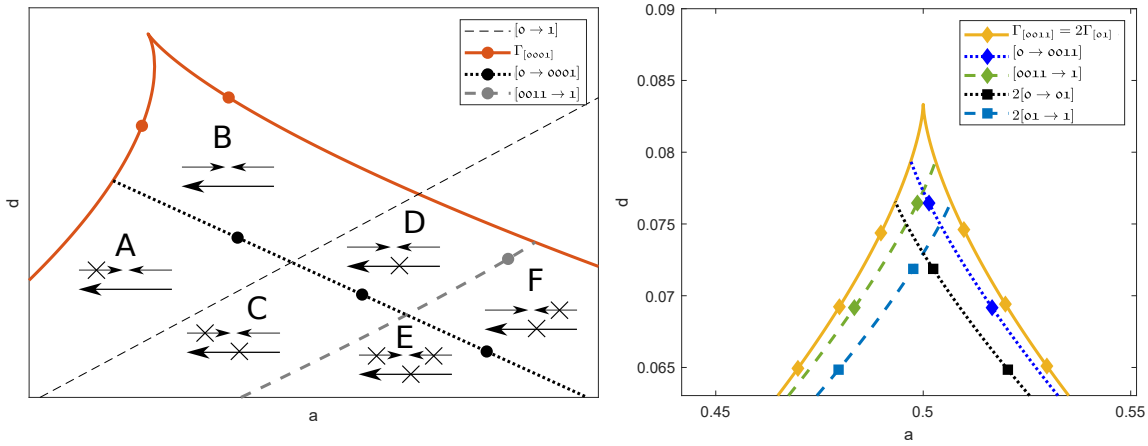

Figure 11: The left panel contains a schematic exaggeration of the area around the cusp of $\Gamma_{[0001]}$, together with a description of the collision type that can be expected in each region. The top two arrows indicate the nature of the $[0 \to 0001]$ and $[0001 \to 1]$ connections that move towards each other. The bottom arrow describes whether or not the resulting monochromatic wave is pinned. The right panel compares the speed threshold for the connections involving $[0011]$ with the doubled bichromatic thresholds. One can see that the reduction (4.2) respects the equilibrium structure but not the wave structure of the system.

together with

$$u_{01}\big(a; d_{[01]}(a)\big) = \big(\frac{a}{2}, 1 - \frac{a^2}{4} - \frac{a^3}{8}\big) + O(a^4). \tag{4.13}$$

The $\Gamma_{[0011]}$ threshold The identity (4.3) allows us to write

$$d_{[0011]}(a) = 2d_{[01]}(a) = \frac{a^2}{4} + \frac{a^4}{16} + O(a^5). \tag{4.14}$$

In addition, we can reuse the expressions (4.13) to find

$$u_{0011}\big(a; d_{[0011]}(a)\big) = \big(\frac{a}{2}, \frac{a}{2}, 1 - \frac{a^2}{4} - \frac{a^3}{8}, 1 - \frac{a^2}{4} - \frac{a^3}{8}\big) + O(a^4). \tag{4.15}$$

The $\Gamma_{[0001]}$ threshold The symmetries discussed above allow us to consider solutions where the first and third component are equal. In particular, we consider the problem

$$G\big((x, y, x, 1 + z); a, d\big) = 0, \tag{4.16}$$

which can be written as

$$(H_1, H_2, H_3)(x, y, z; a, d) = 0 \tag{4.17}$$

with

$$\begin{aligned} H_1(x, y, z; a, d) &= d(y + z + 1 - 2x) + x(1 - x)(x - a), \\ H_2(x, y, z; a, d) &= 2d(x - y) + y(1 - y)(y - a), \\ H_3(x, y, z; a, d) &= 2d(x - z - 1) - z(1 + z)(z + 1 - a). \end{aligned} \tag{4.18}$$

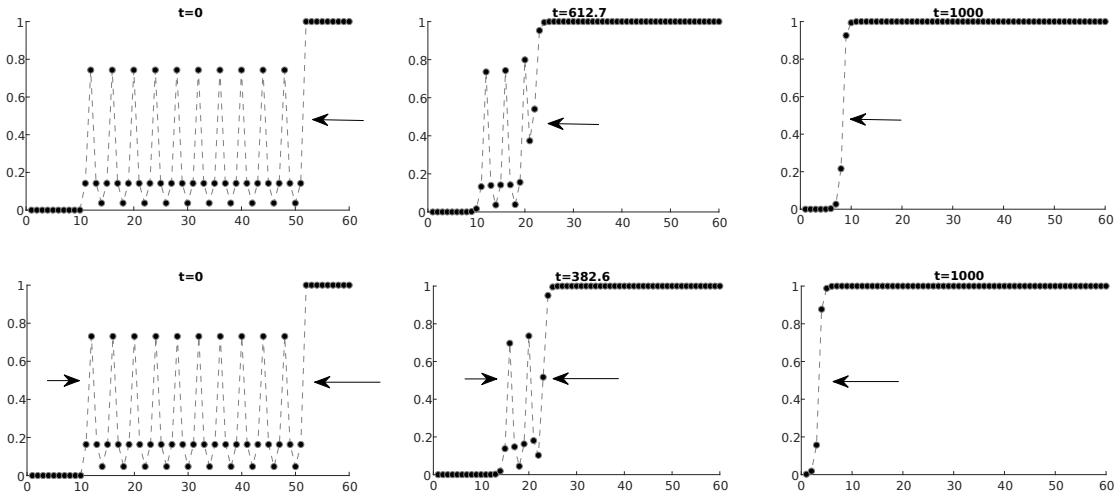

Figure 12: These panels describe two simulations of the LDE (2.1) that feature a collision between a $[\mathtt{0} \to \mathtt{0001}]$ wave and a $[\mathtt{0001} \to \mathtt{1}]$ wave. The top three panels feature a collision of type A, with $a = 0.378$ and $d = 0.058$. The quadrichromatic buffer zone is invaded from the right, forming a travelling monochromatic wave once it is extinguished. The bottom three panels feature a collision of type B, with $a = 0.37$ and $d = 0.0625$. Here the left part of the buffer zone is first pulled towards zero by the incoming wave on the left, but then gets pulled towards one by the final travelling monochromatic wave.

Notice that H_3 features a term of order $O(z)$ and is independent of y. In fact, it is very similar to [24, Eq. (3.30)], which allows us to write

$$z = z_*(x; a, d) = -2d - 2ad + 2dx + O(d^2 + da^2). \tag{4.19}$$

However H_2 features $O\big((a+d)y\big)$ terms, which prevents us from expressing y in terms of x as before. This corresponds with the fact that the root $g(0; a) = 0$ is double at $a = 0$. On the other hand, setting $H_2 = 0$ and introducing the scalings

$$y = a\tilde{y}, \qquad d = d_*(a, \tilde{d}) = \frac{1}{4}a^2(1 + \tilde{d}) \tag{4.20}$$

does allow us to write

$$x = x_*(\tilde{y}; a, \tilde{d}) = a\tilde{y} - \frac{2\tilde{y}}{1 + 4\tilde{d}}(1 - a\tilde{y})(\tilde{y} - 1). \tag{4.21}$$

Substituting these expressions into H_1, we write

$$\tilde{H}_1(\tilde{y}; a, \tilde{d}) = H_1\Big(x_*\big(\tilde{y}; a, \tilde{d}\big), a\tilde{y}, z_*\big(x_*(\tilde{y}; a, \tilde{d}); a, d_*(a, \tilde{d})\big); a, d_*(a, \tilde{d})\Big) \tag{4.22}$$

and find

$$\tilde{H}_1(\tilde{y}; a, \tilde{d}) = 4\tilde{y}^2 + O\big(\tilde{y}^3 + (a + \tilde{d})\tilde{y}^2 + a\tilde{y} + a^2\big). \tag{4.23}$$

The saddle-node bifurcations can now be unfolded by examining the terms in this equation using the procedure in [24]. In particular, we find

$$d_{[\mathtt{0001}]}(a) = \frac{a^2}{4} + \frac{a^3}{8} + O(a^4), \tag{4.24}$$

together with

$$\mathrm{u}_{\mathfrak{oooa}}\big(a; d_{[\mathfrak{oooa}]}(a)\big) = \big(\frac{a}{2} + \frac{a^2}{8} + \frac{3a^3}{16}, \frac{a^2}{4} + \frac{a^3}{8}, \frac{a}{2} + \frac{a^2}{8} + \frac{3a^3}{16}, 1 - \frac{a^2}{2} - \frac{a^3}{2}\big) + O(a^4). \tag{4.25}$$

The main point of interest here is that $d_{[\mathfrak{oooa}]}(a)$ contains a cubic term. In fact, our expansion here agrees with the expansion of the formula [27, Eq. (5.1)], which provides a (non-sharp) upper bound for the values of d where monochromatic waves are pinned. As indicated in Figure 10, our numerical results confirm that $\Omega_{[\mathfrak{oooa}]}$ intersects the region in (a, d) space where monochromatic waves can travel.

4.2 Wave connections

As in the trichromatic case, a visual inspection confirms that assumptions (HΩ1), (HΩ2) and (HS) are satisfied. The connections predicted by Theorem 2.2 are depicted in Figure 7. In Figure 10 we provide the numerically computed minimal values for d for which the waves connecting to and from the spatially homogeneous equilibria $[\mathfrak{o}]$ and $[\mathfrak{a}]$ have a non-zero speed. The novel feature here is that there is overlap with the region where the monochromatic $[\mathfrak{o} \to \mathfrak{a}]$ wave has non-zero speed. This allows for situations where the end-product of a collision between two quadrichromatic wave is no longer a pinned monochromatic wave but in fact a travelling monochromatic wave.

The parameter regions where various types of collisions can occur are described in Figure 11. Types C-F closely resemble those encountered in the bichromatic and trichromatic cases. Types A and B are new and indeed feature travelling monochromatic end-products. Two examples with snapshots of such collisions are provided in Figure 12.

5 Proof of Theorem 2.2

Here we provide the proof of our main result, which allows us to establish the existence of wave connections between equilibria by simply comparing their types.

We first show that a pair of distinct ordered stationary solutions cannot have two equal components. Throughout this section we assume that expressions such as $i-1$ or $i+1$ should be evaluated within the modulo arithmetic on indices $\{1, 2, \ldots, n\}$.

Lemma 5.1. *Assume that* $\mathrm{u}, \mathrm{v} \in \mathbb{R}^n$ *satisfy* $G(\mathrm{u}; a, d) = G(\mathrm{v}; a, d) = 0$ *for some pair* $a \in (0, 1)$ *and* $d > 0$. *Assume furthermore that* $\mathrm{u} \leq \mathrm{v}$ *and that* $\mathrm{u}_i = \mathrm{v}_i$ *for some* $i \in \{1, \ldots, n\}$. *Then in fact* $\mathrm{u} = \mathrm{v}$.

Proof. Since $\mathrm{u}_i = \mathrm{v}_i$ we have

$$0 = d(\mathrm{u}_{i-1} - 2\mathrm{u}_i + \mathrm{u}_{i+1}) + g\big(\mathrm{u}_i; a\big) = d(\mathrm{u}_{i-1} - 2\mathrm{v}_i + \mathrm{u}_{i+1}) + g\big(\mathrm{v}_i; a\big) = d(\mathrm{v}_{i-1} - 2\mathrm{v}_i + \mathrm{v}_{i+1}) + g\big(\mathrm{v}_i; a\big), \tag{5.1}$$

which implies that

$$\mathrm{u}_{i-1} + \mathrm{u}_{i+1} = \mathrm{v}_{i-1} + \mathrm{v}_{i+1}. \tag{5.2}$$

Since $\mathrm{u}_{i-1} \leq \mathrm{v}_{i-1}$ and $\mathrm{u}_{i+1} \leq \mathrm{v}_{i+1}$ we obtain $\mathrm{u}_{i-1} = \mathrm{v}_{i-1}$ and $\mathrm{u}_{i+1} = \mathrm{v}_{i+1}$. This argument can subsequently be repeated a number of times to yield $\mathrm{u} = \mathrm{v}$. □

The main ingredient in our proof of Theorem 2.2 is that the ordering of any pair of words from the full set $\{\mathfrak{o}, \mathfrak{a}, \mathfrak{a}\}^n$ and the stable subset $\{\mathfrak{o}, \mathfrak{a}\}^n$ is preserved for the equilibria that have the corresponding types. For example, for $n = 4$ we have the partial ordering

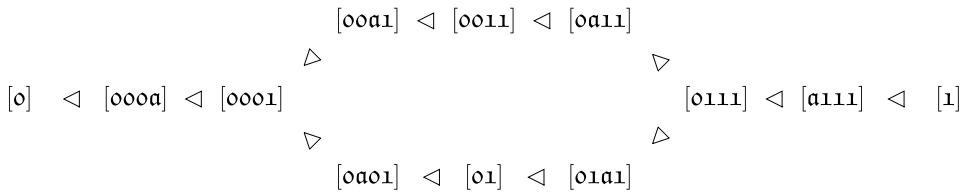

whereby each $[\mathrm{w}_A] \triangleleft [\mathrm{w}_B]$ connection in this diagram indicates that $\mathrm{u}_{\mathrm{w}_A}(a,d) < \mathrm{u}_{\mathrm{w}_B}(a,d)$ whenever $(a,d) \in \Omega_{\mathrm{w}_A} \cap \Omega_{\mathrm{w}_B}$ with $d > 0$.

Lemma 5.2. *Assume that* (HΩ1) *and* (HΩ2) *are satisfied and consider a distinct pair* $\mathrm{w}_A, \mathrm{w}_B \in \{\mathtt{o}, \mathtt{a}, \mathtt{1}\}^n$ *that admits the ordering* $\mathrm{w}_A \le \mathrm{w}_B$. *Suppose furthermore that at least one of these two words is contained in* $\{\mathtt{o}, \mathtt{1}\}^n$. *Then for any* $(a,d) \in \Omega_{\mathrm{w}_A} \cap \Omega_{\mathrm{w}_B}$ *we have the strict component-wise inequality*

$$\mathrm{u}_{\mathrm{w}_A}(a,d) < \mathrm{u}_{\mathrm{w}_B}(a,d). \tag{5.3}$$

Proof. Fixing $(a,d) \in \Omega_{\mathrm{w}_A} \cap \Omega_{\mathrm{w}_B}$, we note that (H$\Omega$1) and (H$\Omega$2) allow us to pick a curve

$$[0,1] \ni t \mapsto \big(\mathrm{v}_A(t), \mathrm{v}_B(t), \alpha(t), \delta(t)\big) \in [0,1]^n \times [0,1]^n \times (0,1) \times [0,\infty) \tag{5.4}$$

so that we have

$$\begin{array}{rcl} (\mathrm{v}_A, \mathrm{v}_B, \alpha, \delta)(0) & = & \big([\mathrm{w}_A]_{|a}, [\mathrm{w}_B]_{|a}, a, 0\big), \\ (\mathrm{v}_A, \mathrm{v}_B, \alpha, \delta)(1) & = & \big(\mathrm{u}_{\mathrm{w}_A}(a,d), \mathrm{u}_{\mathrm{w}_B}(a,d), a, d\big), \end{array} \tag{5.5}$$

while the inclusion

$$\big(\alpha(t), \delta(t)\big) \in \Omega_{\mathrm{w}_A} \cap \Omega_{\mathrm{w}_B} \tag{5.6}$$

and the identities

$$G\big(\mathrm{v}_A(t); \alpha(t), \delta(t)\big) = G\big(\mathrm{v}_B(t); \alpha(t), \delta(t)\big) = 0 \tag{5.7}$$

all hold for $0 \le t \le 1$. By slightly modifying the path and picking a small $\epsilon > 0$, we can also ensure that $\alpha(t) = a$ and $\delta(t) = t$ for all $t \in [0, \epsilon)$.

Upon introducing the graph Laplacian $B : \mathbb{R}^n \to \mathbb{R}^n$ and the nonlinearity $\Psi : \mathbb{R}^n \to \mathbb{R}^n$ that act as

$$(B\mathrm{u})_i = \mathrm{u}_{i-1} - 2\mathrm{u}_i + \mathrm{u}_{i+1}, \qquad \Psi(\mathrm{u})_i = g(\mathrm{u}_i; a), \tag{5.8}$$

we see that

$$0 = G(\mathrm{v}_\#(t); a, t) = tB\mathrm{v}_\#(t) + \Psi\big(\mathrm{v}_\#(t)\big) \tag{5.9}$$

for t small and $\# \in \{A, B\}$. Taking implicit derivatives of (5.9), we find

$$tB\frac{d^k}{dt^k}\mathrm{v}_\#(t) + kB\frac{d^{k-1}}{dt^{k-1}}\mathrm{v}_\#(t) + \mathcal{R}^{(k)}_\#(t) = -D\Psi\big(\mathrm{v}_\#(t)\big)\frac{d^k}{dt^k}\mathrm{v}_\#(t), \tag{5.10}$$

in which we have defined

$$\mathcal{R}^{(k)}_\#(t) = \sum_{j=1}^{k-1} \binom{k-1}{j-1} \Big[\frac{d^{k-j}}{dt^{k-j}} D\Psi\big(\mathrm{v}_\#(t)\big)\Big] \frac{d^j}{dt^j}\mathrm{v}_\#(t) \tag{5.11}$$

for $k \ge 2$, setting this expression to zero for $k = 1$.

For any index i we define the quantity

$$\ell_i = \min\{j' \ge 0 : (\mathrm{w}_A)_{i+j'} < (\mathrm{w}_B)_{i+j'} \text{ or } (\mathrm{w}_A)_{i-j'} < (\mathrm{w}_B)_{i-j'}\}, \tag{5.12}$$

which measures the distance to the closest index where w_A and w_B are unequal. We now claim that for any $k \geq 0$ we have

$$\frac{d^k}{dt^k}(\mathrm{v}_A)_i(0) \leq \frac{d^k}{dt^k}(\mathrm{v}_B)_i(0) \tag{5.13}$$

if $\ell_i \geq k$, with the inequality being strict if and only if $\ell_i = k$. For $k = 0$ this is obvious. Assuming this holds for $k-1$, consider any index with $\ell_i \geq k \geq 1$. Our alphabet assumption implies that

$$(\mathrm{w}_A)_i = (\mathrm{w}_B)_i \neq \mathfrak{a}, \tag{5.14}$$

which implies that the ii-component of the two diagonal matrices $D\Psi\big(\mathrm{v}_A(0)\big)$ and $D\Psi\big(\mathrm{v}_B(0)\big)$ are strictly negative; see (2.7). In addition, our induction hypothesis implies that

$$\mathcal{R}_A^{(k)}(0) = \mathcal{R}_B^{(k)}(0). \tag{5.15}$$

By definition, we have

$$\ell_{i\pm1} \geq \ell_i - 1 \geq k - 1. \tag{5.16}$$

In addition, we have $\ell_i = k$ if and only if $\ell_{i+1} = k-1$ or $\ell_{i-1} = k-1$ holds. Our induction hypothesis hence implies

$$\big(B\frac{d^{k-1}}{dt^{k-1}}\mathrm{v}_A(0)\big)_i \leq \big(B\frac{d^{k-1}}{dt^{k-1}}\mathrm{v}_B(0)\big)_i, \tag{5.17}$$

with strict inequality if and only if $\ell_i = k$. Our claim now follows immediately from (5.10).

The argument above shows that $\mathrm{v}_A(t) < \mathrm{v}_B(t)$ for all $t \in (0, \epsilon)$. If (5.3) fails to hold, this hence means that there exists $t_* \in [\epsilon, 1]$ for which $\mathrm{v}_A(t_*) \leq \mathrm{v}_B(t_*)$, with also $\big(\mathrm{v}_A(t_*)\big)_i = \big(\mathrm{v}_B(t_*)\big)_i$ for some $i \in \{1, \ldots, n\}$. Lemma 5.1 now implies $\mathrm{v}_A(t_*) = \mathrm{v}_B(t_*)$ and hence

$$\mathrm{u}_{\mathrm{w}_A}\big(\alpha(t_*), \delta(t_*)\big) = \mathrm{u}_{\mathrm{w}_B}\big(\alpha(t_*), \delta(t_*)\big), \tag{5.18}$$

which violates Corollary 2.1. □

By combining Lemma's 5.1 and 5.2 we can control all the (marginally) stable equilibria in the box $[\mathrm{u}_{\mathrm{w}_-}, \mathrm{u}_{\mathrm{w}_+}]$. This allows us to finally prove our main result.

Proof of Theorem 2.2. Pick any distinct pair $\mathrm{w}_\pm \in \{\mathfrak{0}, \mathfrak{1}\}^n$ with $\mathrm{w}_- \leq \mathrm{w}_+$ and any $(a, d) \in \Omega_{\mathrm{w}_-} \cap \Omega_{\mathrm{w}_+}$ with $d > 0$. Lemma 5.2 implies that the cuboid

$$\mathcal{K} = \{\mathrm{u} \in \mathbb{R}^n : \mathrm{u}_{\mathrm{w}_-}(a, d) \leq \mathrm{u} \leq \mathrm{u}_{\mathrm{w}_+}(a, d)\} \subset [0, 1]^n \tag{5.19}$$

has non-empty volume. In addition, for any $\mathrm{w} \in \{\mathfrak{0}, \mathfrak{1}\}^n$ that does not satisfy $\mathrm{w}_- \leq \mathrm{w} \leq \mathrm{w}_+$ and for which $(a, d) \in \overline{\Omega}_{\mathrm{w}}$, we have $u_{\mathrm{w}}(a, d) \notin \mathcal{K}$ on account of Lemma 5.1, the connectedness of $\Omega_{\mathrm{w}_\pm} \cap \Omega_{\mathrm{w}}$ and continuity considerations.

In view of (HS), all equilibria inside the cube $\mathcal{K}$ besides the two corner points $\mathrm{u}_{\mathrm{w}_\pm}(a, d)$ hence have a strictly positive eigenvalue. The existence of the wave (c, Φ) now follows from [10, Thm. 6]. □

References

[1] D. G. Aronson and H. F. Weinberger (1975), Nonlinear diffusion in population genetics, combustion, and nerve pulse propagation. In: *Partial differential equations and related topics.* Springer, pp. 5–49.

[2] P. W. Bates and A. Chmaj (1999), A Discrete Convolution Model for Phase Transitions. *Arch. Rational Mech. Anal.* **150**, 281–305.

[3] T. Bellsky, A. Doelman, T. J. Kaper and K. Promislow (2013), Adiabatic stability under semi-strong interactions: the weakly damped regime. *Indiana University Mathematics Journal* pp. 1809–1859.

[4] J. Blot (1991), On global implicit functions. *Nonlinear Analysis: Theory, Methods & Applications* **17**(10), 947–959.

[5] M. Brucal-Hallare and E. S. Van Vleck (2011), Traveling Wavefronts in an Antidiffusion Lattice Nagumo Model. *SIAM J. Appl. Dyn. Syst.* **10**, 921–959.

[6] J. W. Cahn, J. Mallet-Paret and E. S. Van Vleck (1999), Traveling Wave Solutions for Systems of ODE's on a Two-Dimensional Spatial Lattice. *SIAM J. Appl. Math.* **59**, 455–493.

[7] J. W. Cahn and A. Novick-Cohen (1994), Evolution Equations for Phase Separation and Ordering in Binary Alloys. *J. Stat. Phys.* **76**, 877–909.

[8] J. W. Cahn and E. S. Van Vleck (1999), On the Co-existence and Stability of Trijunctions and Quadrijunctions in a Simple Model. *Acta Materialia* **47**, 4627–4639.

[9] V. Celli and N. Flytzanis (1970), Motion of a screw dislocation in a crystal. *Journal of Applied Physics* **41**(11), 4443–4447.

[10] X. Chen, J. S. Guo and C. C. Wu (2008), Traveling Waves in Discrete Periodic Media for Bistable Dynamics. *Arch. Ration. Mech. Anal.* **189**, 189–236.

[11] M. Chirilus-Bruckner, A. Doelman, P. van Heijster and J. D. Rademacher (2015), Butterfly catastrophe for fronts in a three-component reaction–diffusion system. *Journal of Nonlinear Science* **25**(1), 87–129.

[12] S. V. Dmitriev, K. Abe and T. Shigenari (2000), Domain wall solutions for EHM model of crystal:: structures with period multiple of four. *Physica D: Nonlinear Phenomena* **147**(1-2), 122–134.

[13] A. Doelman, T. J. Kaper and K. Promislow (2007), Nonlinear asymptotic stability of the semistrong pulse dynamics in a regularized Gierer–Meinhardt model. *SIAM Journal on Mathematical Analysis* **38**(6), 1760–1787.

[14] C. E. Elmer (2006), Finding Stationary Fronts for a Discrete Nagumo and Wave Equation; Construction. *Physica D* **218**, 11–23.

[15] C. E. Elmer and E. S. Van Vleck (2002), A Variant of Newton's Method for the Computation of Traveling Waves of Bistable Differential-Difference Equations. *J. Dyn. Diff. Eq.* **14**, 493–517.

[16] C. E. Elmer and E. S. Van Vleck (2005), Spatially Discrete FitzHugh-Nagumo Equations. *SIAM J. Appl. Math.* **65**, 1153–1174.

[17] T. E. Faver (2017), Nanopteron-stegoton traveling waves in spring dimer Fermi-Pasta-Ulam-Tsingou lattices. *arXiv preprint arXiv:1710.07376*.

[18] T. E. Faver and J. D. Wright (2018), Exact Diatomic Fermi–Pasta–Ulam–Tsingou Solitary Waves with Optical Band Ripples at Infinity. *SIAM Journal on Mathematical Analysis* **50**(1), 182–250.

[19] P. C. Fife and J. B. McLeod (1977), The approach of solutions of nonlinear diffusion equations to travelling front solutions. *Arch. Ration. Mech. Anal.* **65**(4), 335–361.

[20] T. Gallay, E. Risler et al. (2007), A variational proof of global stability for bistable travelling waves. *Differential and integral equations* **20**(8), 901–926.

[21] A. Hoffman and J. Mallet-Paret (2010), Universality of Crystallographic Pinning. *J. Dyn. Diff. Eq.* **22**, 79–119.

[22] A. Hoffman and J. D. Wright (2011), Exit manifolds for lattice differential equations. *Proc. Roy. Soc. Edinburgh Sect. A* **141**(1), 77–92.

[23] A. Hoffman and J. D. Wright (2017), Nanopteron solutions of diatomic Fermi–Pasta–Ulam–Tsingou lattices with small mass-ratio. *Physica D: Nonlinear Phenomena* **358**, 33–59.

[24] H. J. Hupkes, L. Morelli and P. Stehlík (2018), Bichromatic travelling waves for lattice Nagumo equations. *arXiv preprint arXiv:1805.10977.*

[25] H. J. Hupkes, D. Pelinovsky and B. Sandstede (2011), Propagation failure in the discrete Nagumo equation. *Proc. Amer. Math. Soc.* **139**(10), 3537–3551.

[26] H. J. Hupkes and S. M. Verduyn-Lunel (2005), Analysis of Newton's Method to Compute Travelling Waves in Discrete Media. *J. Dyn. Diff. Eq.* **17**, 523–572.

[27] J. P. Keener (1987), Propagation and its Failure in Coupled Systems of Discrete Excitable Cells. *SIAM J. Appl. Math.* **47**, 556–572.

[28] J. Mallet-Paret (1996), Spatial Patterns, Spatial Chaos and Traveling Waves in Lattice Differential Equations. In: *Stochastic and Spatial Structures of Dynamical Systems*, Royal Netherlands Academy of Sciences. Proceedings, Physics Section. Series 1, Vol. 45. Amsterdam, pp. 105–129.

[29] J. Mallet-Paret (1999), The Global Structure of Traveling Waves in Spatially Discrete Dynamical Systems. *J. Dyn. Diff. Eq.* **11**, 49–128.

[30] J. Mallet-Paret (2001), Crystallographic Pinning: Direction Dependent Pinning in Lattice Differential Equations. *Preprint.*

[31] Y. Morita and H. Ninomiya (2006), Entire solutions with merging fronts to reaction–diffusion equations. *Journal of Dynamics and Differential Equations* **18**(4), 841–861.

[32] Y. Morita and K. Tachibana (2009), An entire solution to the Lotka–Volterra competition-diffusion equations. *SIAM Journal on Mathematical Analysis* **40**(6), 2217–2240.

[33] Y. Nishiura, T. Teramoto and K.-I. Ueda (2003), Scattering and separators in dissipative systems. *Physical Review E* **67**(5), 056210.

[34] P. Poláčik (2016), Propagating terraces and the dynamics of front-like solutions of reaction-diffusion equations on R. *Mem. Amer. Math. Soc., to appear.*

[35] L. A. Ranvier (1878), *Lećons sur l'Histologie du Système Nerveux, par M. L. Ranvier, recueillies par M. Ed. Weber.* F. Savy, Paris.

[36] D. Sattinger (1977), Weighted norms for the stability of traveling waves. *Journal of Differential Equations* **25**(1), 130–144.

[37] W. Schouten and H. Hupkes (2018), Nonlinear stability of pulse solutions for the discrete FitzHugh-Nagumo equation with infinite-range interactions. *arXiv preprint arXiv:1807.11736.*

[38] P. Stehlík (2017), Exponential number of stationary solutions for Nagumo equations on graphs. *J. Math. Anal. Appl.* **455**(2), 1749–1764.

[39] A. Vainchtein and E. S. Van Vleck (2009), Nucleation and Propagation of Phase Mixtures in a Bistable Chain. *Phys. Rev. B* **79**, 144123.

[40] A. Vainchtein, E. S. Van Vleck and A. Zhang (2015), Propagation of periodic patterns in a discrete system with competing interactions. *SIAM Journal on Applied Dynamical Systems* **14**(2), 523–555.

[41] P. van Heijster, A. Doelman, T. J. Kaper and K. Promislow (2010), Front interactions in a three-component system. *SIAM Journal on Applied Dynamical Systems* **9**(2), 292–332.

[42] H. F. Weinberger (1979), Genetic wave propagation, convex sets, and semi-infinite programming. In: *Constructive approaches to mathematical models (Proc. Conf. in honor of R. J. Duffin, Pittsburgh, Pa., 1978).* New York: Academic Press, pp. 293–317.

[43] H. Yagisita (2003), Backward global solutions characterizing annihilation dynamics of travelling fronts. *Publications of the Research Institute for Mathematical Sciences* **39**(1), 117–164.